SU-SEL-66-087

A Crystal Field Analysis of Cobalt Impurities in GaP

by

D. H. Loescher

FACILITY FORM 602
N67-19925 (ACCESSION NUMBER) (THRU) 1
16 (PAGES) (CODE)
CR-82965 (NASA CR OR TMX OR AD NUMBER) 26 (CATEGORY)

October 1966

Technical Report No. 5109-2

Prepared under
National Aeronautics and Space Administration
Research Grant No. NsG-555

SOLID-STATE ELECTRONICS LABORATORY

STANFORD ELECTRONICS LABORATORIES

STANFORD UNIVERSITY • STANFORD, CALIFORNIA

Requests for copies of this report should be referred to:

National Aeronautics and Space Administration
Office of Scientific and Technical Information
Washington, D.C. 20546
Attn: AFSS-A

NOTICE

This report was prepared as an account of Government-sponsored work. Neither the United States nor the National Aeronautics and Space Administration (NASA), nor any person acting on behalf of NASA:

A. Makes any warranty or representation expressed or implied with respect to the accuracy, completeness, or usefulness of the information contained in this report or that the use of any information, apparatus, method, or process disclosed in this report may not infringe privately-owned rights; or

B. Assumes any liabilities with respect to the use of, or for damages resulting from the use of any information, apparatus, method, or process disclosed in this report.

As used above, "person acting on behalf of NASA" includes any employee or contractor of NASA or employee of such contractor, to the extent that such employee or contractor of NASA, or employees of such contractor prepares, disseminates, or provides access to, any information pursuant to his employment or contract with NASA, or his employment with such contractor.

1657

SEL-66-087

A CRYSTAL FIELD ANALYSIS OF COBALT IMPURITIES IN GaP

by

D. H. Loescher

October 1966

Reproduction in whole or in part
is permitted for any purpose of
the United States Government.

Technical Report No. 5109-2

Prepared under
National Aeronautics and Space Administration
Research Grant No. NsG-555

Solid-State Electronics Laboratory
Stanford Electronics Laboratories
Stanford University Stanford, California

ABSTRACT

Crystal field theory has been used to explain the electrical and optical properties of cobalt-doped GaP. In n-type GaP, cobalt gives rise to optical absorption bands at 0.8 and 1.25 microns. From Hall effect data it has been found that cobalt is a deep acceptor with an ionization energy of 0.41 eV. A crystal field analysis has shown that the electron configuration around full cobalt acceptors (negatively charged) consists of seven d-electrons with all other electrons in closed shells, and furthermore, that cobalt atoms have substituted for gallium atoms in the lattice. In general, the analysis has shown that crystal field theory can be used to obtain detailed electron models of semiconductor impurities.

In the course of the study, methods were developed to grow epitaxial single crystals of GaP doped with either sulfur or zinc. Predictable sulfur dopings between 6×10^{16} and 4×10^{18} cm^{-3} were achieved. Radiotracer diffusions were used to introduce a known concentration of cobalt into the samples used for optical and electrical measurements. Diffusion data show that the cobalt diffused both substitutionally and interstitially. The data suggest that the cobalt concentration after diffusion was determined by a nonequilibrium density of crystal defects. This hypothesis is consistent with the conclusion from the optical data that the cobalt was on gallium sites.

CONTENTS

CONTENTS (Continued)

TABLES

ILLUSTRATIONS

ILLUSTRATIONS (Continued)

SYMBOLS

Atomic

s, p, d, f	atomic one-electron wave functions
^4_F, ^4_P	LS-coupled many-electron wave functions

Symmetry

A_1, A_2, E, T_1, T_2	Mulliken's notation for the irreducible representations of the tetrahedral group
$^4A_2$, $^4T_1$, $^4T_2$	quartet tetrahedral field levels

General

A, B, C	Racah parameters (energy units)
c	counting rate, above background
C_B	number of background counts
C_T	total number of counts
[Co]	cobalt concentration (atoms/cm^3)
D	diffusion coefficient (cm^2/sec)
Dq	crystal field parameter (energy units)
E	energy
E_A	acceptor ionization energy
E'_A	$E_A + kT \ln \gamma$
E_F	Fermi energy
E_F^o	Fermi energy extrapolated to T = 0
E_S	sulfur ionization energy
k	Boltzmann's constant
kT	thermal energy

H	Hamiltonian
m_h	effective mass of holes
N_A	total density of acceptors (cm^{-3})
N_A^o	density of neutral acceptors (cm^{-3})
N_A^-	density of negative acceptors (cm^{-3})
n	electron concentration (cm^{-3})
n_i	intrinsic carrier concentration (cm^{-3})
N_d	total donor density (cm^{-3})
N_d^o	density of neutral donors (cm^{-3})
N_d^+	density of positive donors (cm^{-3})
N_V	density of valence band states (cm^{-3})
N_V'	$N_V T^{3/2}$
p	hole concentration (cm^{-3})
R_H	Hall coefficient (cm^3/coulomb)
t	thickness of a lapped layer (cm)
T	temperature (°K unless otherwise indicated)
U	potential energy
Δw	weight removed while lapping (grams)
α	absorption coefficient (cm^{-1})
β	temperature coefficient of the Fermi energy
γ	electron degeneracy factor
μ	mobility (cm^2/volt sec)
ζ	spin-orbit interaction parameter (energy units)
ρ	resistivity (ohm-cm)
ρ_{GaP}	density of GaP

ACKNOWLEDGMENT

The author wishes to thank Professors G. L. Pearson, J. L. Moll, and D. A. Stevenson for their guidance and encouragement. Particular thanks are due Professor J. W. Allen for suggesting the problem and for countless patient discussions.

Financial support was provided by the National Aeronautics and Space Administration. The author used facilities provided by the Advanced Research Projects Agency through the Center for Materials Research at Stanford University.

I. INTRODUCTION

Semiconductor impurities are technologically important because they can control the resistivity, lifetime, photoresponse, etc., of a semiconductor. Much research has been done on shallow impurities, particularly in silicon and germanium, and such impurity levels are now quite well understood. Deep impurity levels have also been studied extensively but they are not well understood. A major difficulty has been the lack of a theoretical framework in which to put empirical results. It now appears that a phenomenological theory for transition-metal impurities may provide a suitable framework.

Allen [Ref. 1] has suggested that transition-metal impurities can be understood in terms of an extension of crystal field theory. Since the 3d shell is shielded by outer electrons, the effect of the crystalline environment on the 3d orbitals can be treated as a perturbation on well-understood free atom wave functions. Crystal field theory was developed specifically to calculate the perturbed 3d shell wave functions. Experimentally the structure of the 3d shell can be determined by observing transitions within the shell. By comparing the crystal field calculations with the observed structure, the number of 3d electrons and the symmetry of the impurity site can be determined. A knowledge of the number of 3d electrons and of the site symmetry can then be used to develop a detailed picture of the electron configuration around the impurity.

Crystal field theory has been used in the past to study transition-metal impurities in II-VI compounds, but no attempt was made to correlate the results with the electrical properties of the impurity [Refs. 2,3]. Allen showed that it would be possible to correlate crystal field and electrical data. The purpose of this work is to show through a detailed experimental investigation how such a correlation can be done.

In order to demonstrate the method, the properties of cobalt-doped gallium phosphide were studied in detail. There were a number of reasons for the decision to study cobalt impurities in the GaP lattice. First, the band gap of GaP is wide enough so that cobalt-impurity absorption is not masked by band-edge absorption. Second, it proved possible to grow large single crystals of both n-type and p-type GaP. Finally, crystal

field theory had not been applied previously to a material as covalent as GaP. Cobalt was chosen because it has a distinctive absorption spectrum in GaP and because its concentration in the crystals could be determined through the use of cobalt-60. The latter has a 5.2-year half-life which is convenient for radiotracer work.

This study of cobalt in GaP involved four essentially independent experiments. It was necessary to grow crystals of GaP because high-quality GaP was not commercially available. Radiotracer diffusions were used to introduce known concentrations of cobalt into the grown crystals. Cobalt was not introduced during crystal growth because radiotracers could not be used safely in the growth system. Hall effect measurements and optical transmission work provided the information necessary to demonstrate the crystal field method.

II. THEORETICAL BACKGROUND

In this chapter the elements of impurity theory used in this work are reviewed. Impurity theory in general, the theory of transition-metal impurities, and the theory developed by Allen [Ref. 1] are discussed.

A. GENERAL IMPURITY THEORY

In order to calculate the ionization energy, photoresponse, recombination action, etc. of an impurity, it is necessary to know the impurity wave functions. In principle, the wave functions can be found by comparing the eigenfunctions of the Hamiltonian for a perfect crystal plus one impurity, with those of the Hamiltonian for a perfect crystal. The presence of the impurity gives rise to localized electronic modes that do not exist in the pure crystal. In practice, it is extremely difficult to find the eigenfunctions of a pure crystal and it is virtually impossible to find those of an impure crystal.

Impurity wave functions can sometimes be determined by perturbation calculations for the cases of either very loose or very tight binding. The perturbation calculations have been approached either by treating the impurity as a perturbation on the lattice or by treating the lattice as a perturbation on the impurity. In the first method the impurity wave function is expanded in terms of the wave functions of the crystal; whereas in the second, atomic wave functions of the impurity atom are used in the expansion. Since crystal wave functions are unbounded in extent, the first approach is most successful for impurity orbits that are very large. Its greatest success has been with the shallow impurity orbits of germanium. In contrast to the crystal wave functions, atomic wave functions are quite small. The maximum charge density is typically only 0.5 Å to 2 Å from the nucleus [Ref. 4]. Consequently, an expansion in terms of atomic orbitals is most useful for describing very localized electronic states such as 3d and 4f levels. The method has been used extensively in studying the rare earths used in lasers.

Impurities with bindings intermediate between very tight and very loose can be treated approximately by extending either of the two methods just mentioned. The loose-binding method can be extended to handle impurities

with ionization energies up to about 0.1 eV. For impurities with binding energies in excess of 0.1 eV, it appears best to extend the theory of deep impurities.

B. TRANSITION-METAL IMPURITIES

1. Introduction

The transition metals provide a group of impurities on which it is reasonable and possible to carry out an extension of tight-binding methods. The 3d shell is often sufficiently shielded by outer electrons that its wave functions can be calculated by using crystal field theory. On the other hand, the d shell frequently interacts sufficiently with the lattice to give rise to electrically active levels. Tight-binding methods are also applicable to 4f shell impurities, but the f shell is too well shielded to be electrically active.

Many of the electrical levels of the transition metal impurities arise because the metals are chemically similar to the metallic constituents of both the III-V and the II-VI compounds. The free atoms of the transition metals, with the exception of chromium and copper, have $d^n 4s^2$ configurations. The group II and group III elements have electron configurations consisting respectively of two or three electrons outside of closed shells. Hence, when one of the transition metals substitutes for a group II element, the two 4s electrons can be used to fill the bonding orbitals and the d shell can either accept electrons from or supply electrons to the crystal lattice. A transition metal which substitutes for a group III atom in a III-V compound can give rise to two different types of impurity levels. The first type arises because the d shell of the impurity can accept and supply electrons. The second type arises because the transition metal has one less outer electron available for bonding than the group III element it replaces.

As suggested in the preceding paragraph, a study of a transition-metal impurity involves determining (1) if there are impurity wave functions which are essentially the same as atomic d wave functions, i.e., if the impurity has a d shell; (2) if the d shell is responsible for the observed electrical effects of the impurity; and (3) the type of

lattice site that the impurity occupies. If d-like wave functions cannot be assigned to the impurity, then the above approach is not relevant. If the impurity does have a d shell, the answer to (2) can be determined by counting the number of d electrons when the impurity level is full and when it is empty.

As an example, consider the case of an acceptor level. If there are n electrons in the d shell when the level is empty and n+1 electrons when the level is full, then apparently the d shell is responsible for the level. On the other hand, if the number of d electrons is the same whether the level is full or empty, then the acceptor level cannot be attributed to the d shell. Finally, the answer to (3) can sometimes be determined by finding the symmetry of the impurity lattice site. Knowledge of the site symmetry may also be useful in specifying the impurity orbital in case the level cannot be attributed to the d shell.

The necessary information regarding the number of d electrons and the impurity site symmetry can sometimes be obtained by combining optical absorption data and Hall effect data. The impurity ionization energy can be obtained from the latter data. The Hall effect can also be used to determine whether, in a particular sample, the Fermi level is above or below the impurity level. The number of d electrons and the site symmetry can be determined by observing optical transitions within the d shell. The theory needed to determine the structure of the d shell from the optical absorption data is given in the following sections.

2. Crystal Field Theory

The form of crystal field theory used in this work results from the assumption that the effects of the lattice on the d wave functions can be described solely in terms of electrostatic interactions. This assumption is difficult to justify a priori for the III-V compounds, but it is the only one that leads to a mathematically tractable theory. A more comprehensive theory which recognizes the possibility of charge exchange between the impurity and the lattice has been suggested by Ballhausen [Ref. 5], but it is not yet well developed. Progressively more extensive treatments of the material given below may be found in the books by McClure [Ref. 6], Ballhausen [Ref. 5], and Griffith [Ref. 7].

In the electrostatic approximation, the Hamiltonian for an electron on the impurity may be written as

$$H = H_{LS} + V_{X\text{-tal}} \,, \tag{2.1}$$

where H_{LS} stands for all the terms that lead to the familiar LS coupling scheme [Ref. 5, p. 8]. The actual values of the terms in H_{LS} will be reduced from their free ion values, however, because of the screening caused by the lattice. $V_{X\text{-tal}}$ is the coulomb potential at the impurity site due to the atoms surrounding the impurity and hence has the symmetry of the impurity lattice site. The Hamiltonian has a simple form because the electrostatic approximation amounts to treating the atoms of the lattice as point charges.

The dominant terms in H_{LS} lead to the central field approximation. The result of that approximation is that one-electron wave functions exist which can be specified by both an orbital quantum number and an angular momentum quantum number; e.g., 1s, 3d, etc. The wave functions for a many-electron atom are constructed by forming Slater determinantal wave functions (hereafter SDWF) out of the one-electron wave functions. The terms in H_{LS} not included in the central field approximation lead to energy differences among the SDWFs made up of the same elementary wave functions. The energy differences arise from interaction among electrons.

As a specific example, consider the d wave functions for electron configurations consisting of n d-electrons plus closed atomic shells (an empty shell is considered to be a closed shell for the purposes of this discussion). The restriction of closed shells is imposed because they give rise to spherically symmetric potentials and hence cannot cause mixing among d wave functions. The central field approximation leads to 10 independent d wave functions. These functions for a d^n ion are SDWFs made up from groups of n different wave functions selected from among the ten. For $n = 1$ there are 10 such SDWFs, for $n = 2$ there are 45, etc. The SDWFs may conveniently be labeled with the total spin S and the total angular momentum L; for example, ^1S, ^4F. An SDWF with quantum numbers L and S corresponds to $(2L+1) \times (2S+1)$ degenerate wave functions. The relative energies of SDWFs with different values of

L and S can be written in terms of three Racah parameters of electrostatic interaction, A, B, and C [Ref. 7, Chapter 6].

The $V_{X\text{-tal}}$ term in Eq. (2.1) causes the mixing of different SDWFs. Hence the solutions to Eq. (2.1) are linear combinations of the individual SDWFs. The mixing occurs because those SDWFs for the free ion that "point" toward the atoms in the lattice have a different energy from those that point away from the lattice sites. Because of the mixing, L is not a good quantum number in the crystal and must be replaced with a number based on the symmetry group of the lattice. We assume that S is a good quantum number in the crystal.

The matrix elements needed to solve Eq. (2.1) are available for the case of $3d^n$ ions, with all shells except the d shell closed, in cubic crystal fields [Ref. 6, Part II, Chapter 2]. The matrices can be used to calculate the eigenfunctions and eigenvalues of Eq. (2.1) in terms of the Racah parameters B and C and the crystal field parameter Dq. The latter is related to the magnitude of $V_{X\text{-tal}}$. The matrix elements can be used to construct a plot of the eigenvalues of Eq. (2.1) as a function of Dq. It is convenient to calculate the eigenvalues in units of B and to plot them vs Dq/B. Such a plot for d^7 in a tetrahedral field is shown in Fig. 1. Only the lower energy eigenvalues are shown. The eigenvalues of Dq/B = 0 are those of the SDWFs (for C/B = 4.75) of a free ion with configuration d^7.

The following selection rules for electric dipole transitions are used to estimate the absorption spectrum from a plot of d^n eigenvalues. First, the total spin S is conserved in an electric dipole transition. This rule is relaxed by spin-orbit interaction, but is quite good for the 3d ions. Second, there are symmetry selection rules that can be calculated with standard group theoretic methods. Third, electric dipole transitions are forbidden between two pure d states. This rule is relaxed at crystal sites that lack inversion symmetry because the local potential can cause mixing of p and d states. Typical values for the oscillator strengths of transitions at centrosymmetric octahedral sites are 10^{-5} to 10^{-7}, but at tetrahedral sites the values are typically 10^{-2} to 10^{-3}. Magnetic dipole and other higher order transitions are inherently too weak to be important at the low impurity concentrations of interest.

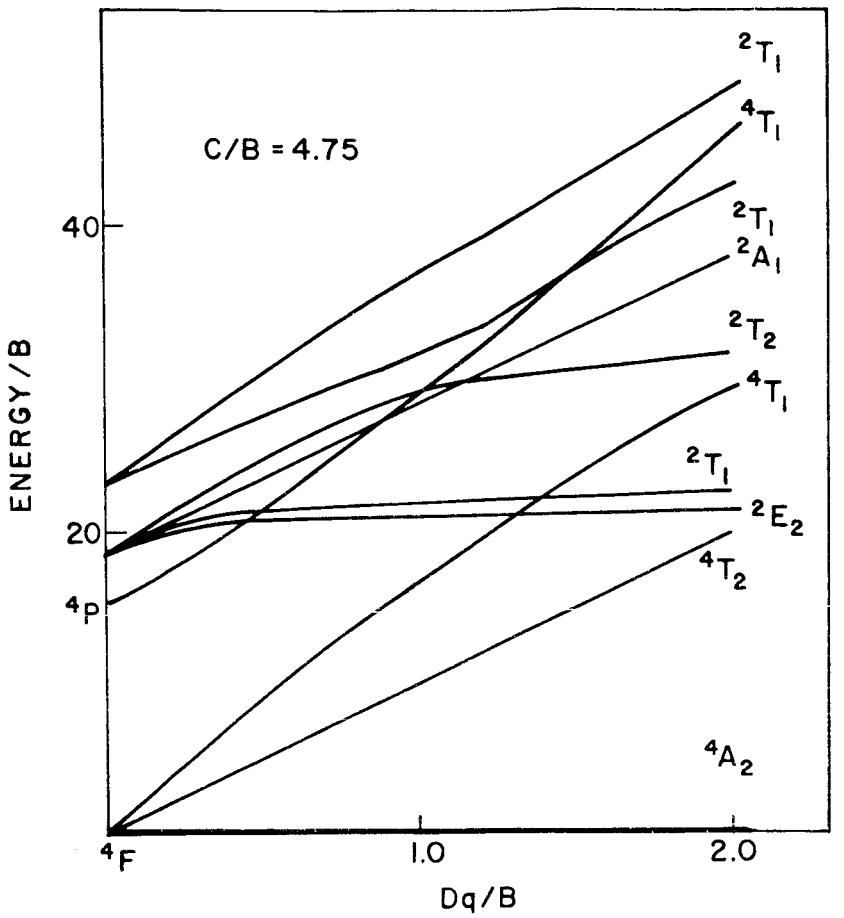

FIG. 1. EIGENVALUE PLOT FOR d^7 IN A TETRAHEDRAL FIELD.

As a concrete example of the use of the matrix elements and the selection rules, consider a d^7 ion in a crystal with the zinc blende structure, e.g., GaP or GaAs. Both the interstitial and the substitutional sites in a zinc blende lattice have tetrahedral symmetry. The symmetry operations of the tetrahedral group T_d are E, $8C_3$, $6\sigma_d$, $6S_4$, and $3C_2$ [Ref. 5, p. 42]. The character table (in Mulliken's notation) of the group is [Ref. 8] shown in Table 1, and the direct product table for the tetrahedral group is shown in Table 2. The symmetry allowed electric dipole transitions can be calculated from Table 2 by using the fact that the dipole moment operator transforms as T_2. The allowed transitions are shown in Table 3, where an "X" means that a transition between the two states is allowed.

TABLE 1. CHARACTER TABLE FOR T_d

	E	$8C_3$	$3C_2$	$6\sigma_d$	$6S_4$
A_1	1	1	1	1	1
A_2	1	1	1	-1	-1
E	2	-1	2	0	0
T_1	3	0	-1	-1	1
T_2	3	0	-1	1	-1

TABLE 2. DIRECT PRODUCT TABLE FOR T_d

	A_1	A_2	E	T_1	T_2
A_1	A_1	A_2	E	T_1	T_2
A_2		A_1	E	T_2	T_1
E			E, A_1, A_2	T_1, T_2	T_1, T_2
T_1				T_1, T_2, E, A_1	T_1, T_2, E, A_2
T_2					T_1, T_2, E, A_1

TABLE 3. ALLOWED DIPOLE TRANSITIONS IN T_d

	A_1	A_2	E	T_1	T_2
A_1					X
A_2				X	
E				X	X
T_1		X	X	X	X
T_2	X		X	X	X

A typical eigenvalue plot for d^7 in a tetrahedral field has been given in Fig. 1. The separation between the crystal field levels is typically much larger than kT (thermal energy) so that only transitions starting at the $^4A_2$ ground state will appear in the absorption spectrum. Reference to Table 3 shows that the only symmetry allowed transitions from an A_2 level are to T_1 levels. The spin selection rule requires that the transitions from $^4A_2$ be to other quartet levels. The only levels that satisfy both requirements are the two quartet $^4T_1$ levels. Hence we predict that the absorption spectrum of a sample containing a d^7 ion on a tetrahedral site will contain two strong peaks. The spectrum will also contain a number of weak peaks due to forbidden transitions from $^4A_2$ levels to levels that are not T_1-like or that are not quartets. If necessary, the spin-orbit splitting of the absorption peaks can also be estimated [Ref. 5, Chapter 6]. A qualitative spectrum can be constructed for any d^n ion in exactly the same way as for the d^7 ion.

3. Application of the Theory

A determination of an impurity's d-shell structure and its site symmetry involves four steps:

1. The optical absorption spectrum of the impurity is measured experimentally.
2. An eigenvalue plot and a qualitative spectrum are constructed for each likely number of d electrons and for each possible site symmetry.

3. The observed spectrum is compared with the calculated spectrums until a likely match is found.

4. An attempt is made to find values of B, C, and Dq for which the calculated energy-level scheme accurately fits the location of the peaks in the observed spectrum.

If a fit cannot be achieved, it must be concluded that the absorption is not due to transitions within the d shell or that a more extensive theory is needed. If a satisfactory fit is achieved, then the number of d electrons and the site are immediately known.

4. Extension of Crystal-Field Theory by Allen

Allen has suggested that impurity ionization energies can sometimes be calculated by the following extension of crystal field theory [Ref. 1]. The energy E_n of the ground state of a d^n configuration may be written as

$$E_n = -nU + \frac{n^2-n}{2} A - b_n B + c_n C + d_n Dq \ , \qquad (2.2)$$

where U is the potential energy of the d electrons in the coulomb field of the core, A, B, and C are the Racah parameters, and Dq is the crystal field parameter. The quantities b_n, c_n, and d_n can be determined from the tabulations of Griffith [Ref. 7, p. 101] and the matrix elements of Tanabe and Sugano [Ref. 9]. More important than the value of E_n is the difference between the value of E_n and the value of E_{n-1}:

$$E_n - E_{n-1} = -U + (n-1) A - (b_n - b_{n-1}) B + (c_n - c_{n-1}) C + (d_n - d_{n-1}) Dq \ . \qquad (2.3)$$

If an impurity level can be attributed to a change from a d^{n-1} to a d^n configuration, the ionization energy of the level should be approximately equal to the energy difference given by Eq. (2.3) [Ref. 10]. The quantities U, A, B, C, and Dq must be determined from experimental data. However, once the five quantities have been determined for two or three members of the d^n series in a particular crystal, it should be possible to estimate the values for the other ions sufficiently accurately to calculate the ionization energies of the entire d^n series. Allen has tried

this sort of extrapolation with considerable success in the II-VI compound ZnS [Ref. 1].

Before Allen's theory can be applied to an impurity level in a III-V compound, it is necessary to show that crystal field theory is applicable to covalent crystals and that the level of interest can be attributed to changes in the d shell of the impurity.

C. SUMMARY

A possible way to treat impurities with intermediate ionization energies is to extend the theories applicable to very tightly bound electronic states. The transition metals provide an interesting and tractable group of impurities on which to try such an extension. The results of a systematic study of the transition metals should provide a framework in which other impurity results can be placed.

In order to apply the existing theories of transition-metal ions to impurities in III-V compounds, it is necessary to show experimentally that the theories are applicable to materials with appreciably equivalent bonds. In order to apply the theory proposed by Allen, it is further necessary to show that the level under investigation can be attributed to the d shell of the impurity.

III. CRYSTAL GROWTH

A. DESCRIPTION OF THE EPITAXIAL SYSTEM

The GaP crystals used in this study were grown in an open-tube epitaxial growth system. The system was originally developed by Gibbons and Prehn [Ref. 11] and was later modified by Chen [Ref. 12]. Either zinc or sulfur was incorporated in the crystals to control their resistivities. Zinc is a shallow acceptor and sulfur is a shallow donor in GaP.

The system is shown schematically in Fig. 2. Tank hydrogen was first purified in a Milton Roy Serfass Hydrogen Purifier† and then fed into three oil manometers. The first manometer metered the hydrogen flow through the PCl_3 bubbler, the second monitored the flow used for sulfur doping, and the third metered the by-pass flow. The flow through each of the three lines was controlled by a precision needle valve. After passing over the reagents, the hydrogen passed through a 2.5-cm I.D. vycor reaction tube in the Marshall furnace.‡ The temperature profile of this furnace was

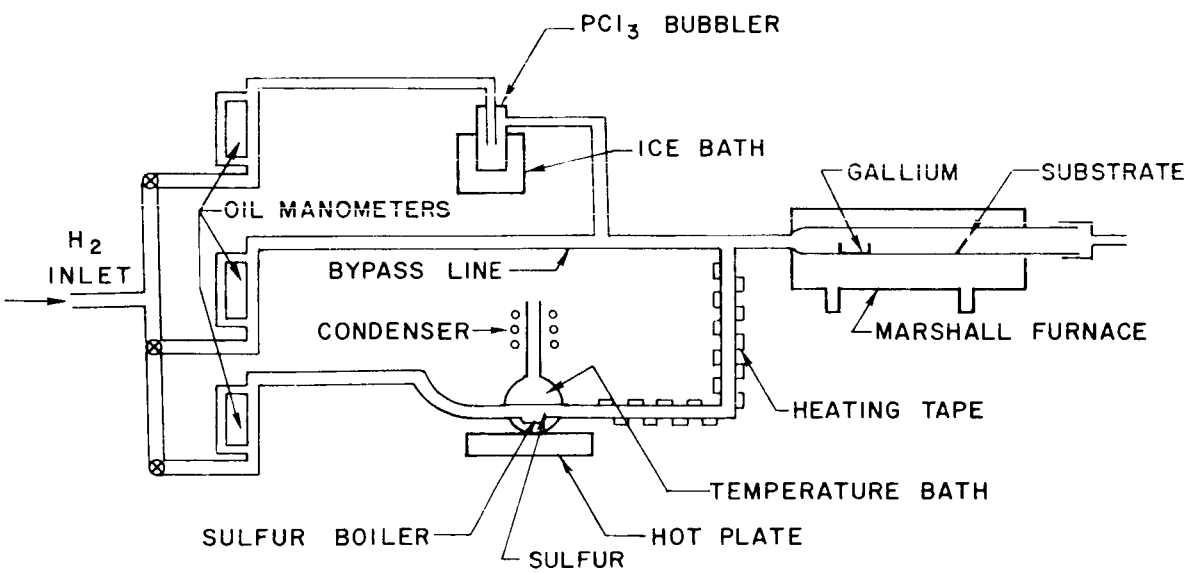

FIG. 2. SCHEMATIC DIAGRAM OF THE APPARATUS USED TO GROW SULFUR-DOPED CRYSTALS.

† Milton Roy Co., Chesterland, Ohio.

‡ Furnace Serial #6110181, Marshall Products Co., Columbus, Ohio.

adjusted with external resistance shunts so that the gallium metal was maintained at 970 °C and the substrate was at 805 to 820 °C. The gas stream picked up gallium at the boat and deposited GaP on the GaAs seed. Wastes from the chemical reactions were deposited at the far end of the tube, and the hydrogen was burned off at the exit.

A qualitative picture of the transport mechanism is given by the following chemical equations, which have not been verified experimentally [Refs. 11,12]:

At 970 °C	$4PCl_3 \rightarrow P_4+12Cl$
	$Cl+Ga \rightarrow GaCl$
At 805 - 820 °C	$2GaCl+H_2 \rightarrow 2HCl+2Ga$
	$4Ga+P_4 \rightarrow 4GaP$
At the exit end of the furnace	$3GaCl \rightarrow GaCl_3+2Ga$

The major waste of the system is $GaCl_3$, which tends to clog the reaction tube; this limits the amount of crystal that can be grown in a single run.

The crystals were doped by introducing either sulfur or zinc into the gas stream. The sulfur was introduced by passing part of the hydrogen flow over solid sulfur that was maintained at constant temperature by a bath of boiling liquid.† Sulfur is the only one of the common n-type GaP dopants for which a simple and reliable boiling-liquid temperature control was found convenient. Zinc doping was accomplished by adding a minute quantity of zinc metal to the gallium.

B. EXPERIMENTAL

1. Methods and Conditions of Growth

In preparation for growth, the PCl_3 bubbler was cleaned with HCl and then rinsed with methanol and dried. The reaction tube and the boat (Fig. 3) were soaked in aqua regia for from 5 to 24 hours and then rinsed with deionized water and methanol. The cleaned reaction tube and boat

†Acetone, methanol, and water were used.

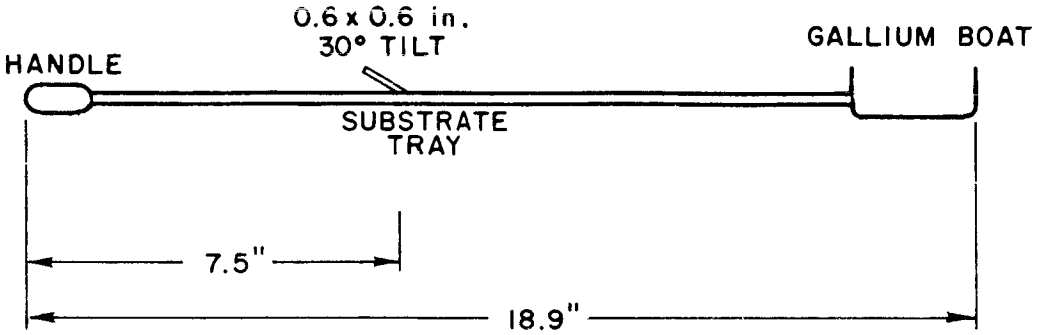

FIG. 3. GALLIUM BOAT AND SEED HOLDER USED IN CRYSTAL GROWTH.

were coated with carbon in the regions where GaP would be deposited. Strains caused by differences in the thermal expansion of quartz and GaP caused uncoated tubes and boats to break. The carbon coating also made it easier to remove the grown crystal and to clean the quartz. The reaction tube was coated in the furnace by cracking methane and the boat was coated in a Bunsen burner flame. The tube was kept hot from the time it was coated until growth was started. An argon flow was used to prevent oxidation of the carbon.

The furnace temperature profiles used during growth are shown in Fig. 4. Profile 1 was used for crystals S1 through S8, and profile 2 was used for the remaining crystals. Aging of the furnace necessitated this change in profile. The temperature range within which the substrates were located is also indicated on Fig. 4. The higher temperatures were used to grow undoped crystals and the lower temperatures were used to grow doped crystals. When the seed was located in the range shown, there was a temperature difference of about 10 °C between its downstream edge and its upstream edge. If the seed was properly located, the 10 °C temperature difference did not interfere with the growth of a crystal of nearly uniform thickness.

The GaAs wafers used for substrates were obtained from the Monsanto Chemical Co.[†] in the form of $\langle 111 \rangle$ oriented slices cut from an undoped boule. The first step in the preparation of the wafers was the determination of the gallium and phosphorus faces either from data supplied by Monsanto or from an orientation etch [Ref. 13]. Second, the wafers were

[†]Monsanto Chemical Co., St. Louis, Missouri.

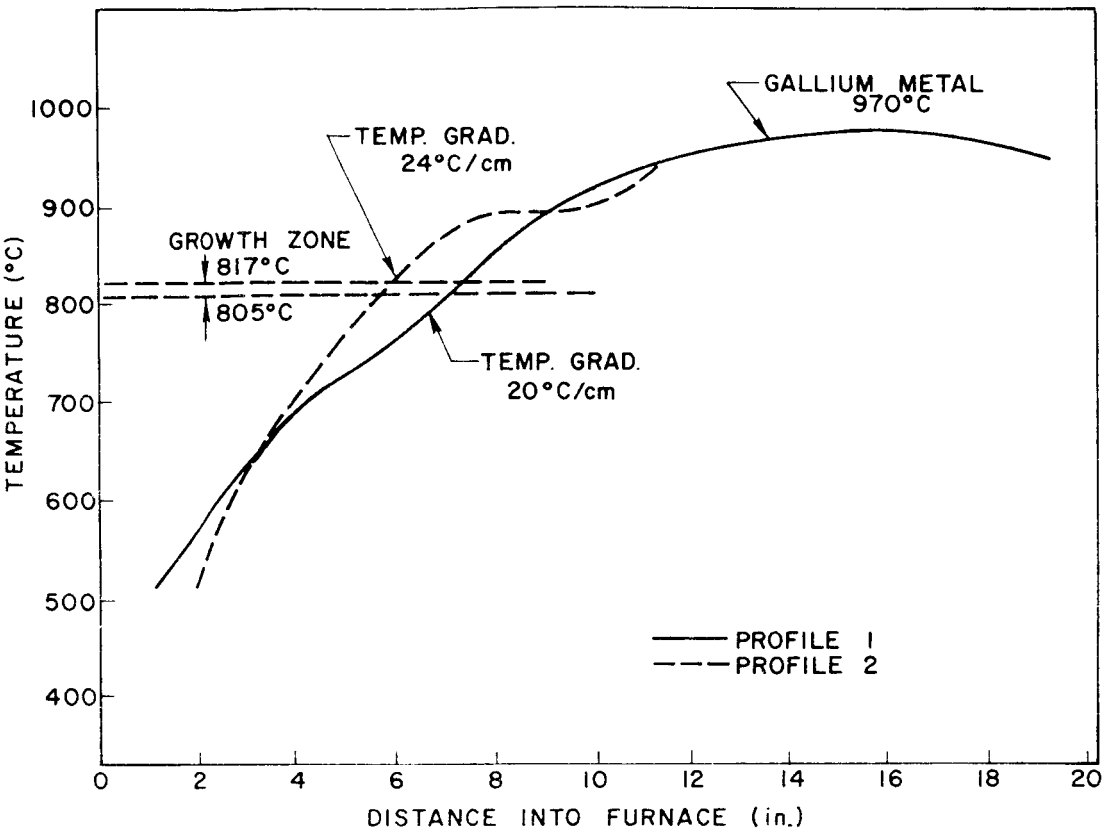

FIG. 4. TEMPERATURE PROFILES FOR THE CRYSTAL-GROWTH FURNACE.

lapped with 3200 grit carborundum powder and then etched in $9HNO_3$:1HF:10 H_2O for from 2 to 5 minutes. Etched samples were stored under methanol in order to prevent oxidation. Notice that the substrates were not polished before use.

Gallium, PCl_3, sulfur, and zinc were used as purchased. Gallium metal of seven nines purity was obtained from the Eagle-Picher Company; PCl_3, reagent grade, and sulfur, U.S.P. grade, were obtained from the Baker Adamson Company; and zinc metal of five nines purity, in the form of 1-mg disks, was purchased from Cominco.†

When the preparations for growth were complete, the GaAs substrate was removed from its methanol storage bath and put, gallium face up, on the substrate holder. Next, approximately 8 gm of gallium metal were put

†Eagle-Picher Co., Quapaw, Oklahoma; Baker Adamson, Division of Allied Chemical and Dye Corp., New York, N.Y.; and Cominco Metals, Inc., Spokane, Washington.

into the quartz boat. The seed and the gallium were then placed in the furnace. A large argon flow was used to prevent oxygen from entering the furnace while the boat was being inserted.

After the boat was inserted, the argon flow was shut off and the hydrogen flow was started. A total flow of 140 to 150 cc/min was found best for the 2.5-cm I.D. reaction tube. The total hydrogen flow was made up of three parts. The first part consisted of 52 cc/min that had passed through PCl_3 maintained at 0 °C. This flow of 52 cc/min transported 1.0×10^{-4} moles of phosphorus/min. Larger phosphorus flows led to poor crystal quality and smaller flows reduced the growth rate. The second part was used for sulfur doping. The third part was added to maintain the total flow between 140 and 150 cc/min.

2. Methods of Estimating Doping Levels

Estimates of the conditions needed to grow a crystal containing a given concentration of sulfur or zinc were made as follows. The possibility of chemical reaction between the dopant and the reagents used to grow the crystal was ignored. For sulfur doping it was assumed (1) that the hydrogen that passed over the solid sulfur was saturated with sulfur vapor, and (2) that the ratio of sulfur atoms to phosphorus atoms would be the same in the grown crystal as it had been in the gas stream. The composition of the zinc-gallium solution used to grow the one zinc-doped crystal was 2 parts zinc to 10^7 parts gallium. This ratio was chosen for a doping of 1.4×10^{17} cm^{-3}. In the estimate it was assumed (1) that the zinc vapor pressure over the zinc-gallium solution was 2×10^{-7} times less than the vapor pressure of pure zinc, and (2) that the ratio of zinc to phosphorus would be the same in the crystal as it had been in the gas stream.

3. Electrical Measurements Performed on the Crystals

Hall coefficient and resistivity were measured on eight sulfur-doped crystals, on the zinc-doped crystal, and on an undoped crystal. Measurements were made on rectangular bars cut from the crystals. The sulfur-doped bars were cooled to liquid nitrogen temperature and then measured as they warmed up. (Electrical contact to the bars was made with tin contacts which were alloyed to the bars in a hydrogen furnace.)

The undoped crystal and the zinc-doped one were measured in the Hall effect apparatus described in Chapter V.

C. RESULTS OF CRYSTAL GROWTH

Data from the crystal growths carried out in the study are summarized in Table 4. Of the 23 growths performed, 21 yielded some single crystalline material and 2 failed due to improper location of the seed. Typically, the result of an 8-hour growth was a 1-cm^2 single crystal between 500 and 700 microns thick.

The Hall effect data for crystals S1, S5, S6, S8, and S11 are given in Fig. 5. The shape of the plots suggests that the samples contain only sulfur donors or that they contain sulfur donors and a compensating impurity. The data for crystals S2, S3, and S4 as given in Fig. 6, suggest that these three samples contain sulfur and another very shallow donor. There is nothing about the growth conditions of the crystals that explains why the two different types of plots shown in Figs. 5 and 6 were obtained. Typical mobility data from the sulfur-doped crystals are shown in Fig. 7.

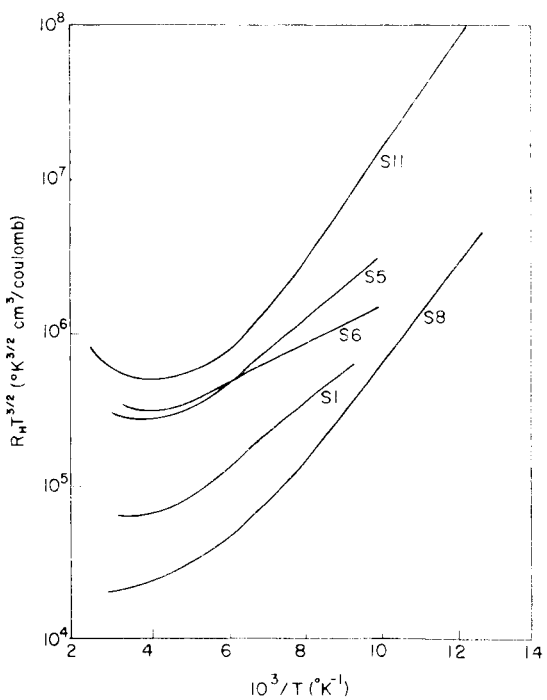

FIG. 5. THE HALL COEFFICIENT TIMES $T^{3/2}$ VS $10^3/T$ FOR FIVE DIFFERENT SULFUR-DOPED GaP CRYSTALS.

TABLE 4. GaP CRYSTAL GROWTH DATA

Crystal	Sulfur Flow† (moles/min)	P Flow (moles/min)	Expected Doping Level (carriers/cm^3)	Electrons/cm^3 at 300 °K	Hall Mobility (cm^2/volt sec)	Comments‡
S0	Undoped	1.0×10^{-4}	---	10^6 ohm - cm		Very thin crystal
S1	M 2.0×10^{-9}	1.0×10^{-4}	5×10^{17}	5×10^{17}	130	Average
S2	M 4.9×10^{-10}	1.0×10^{-4}	1.2×10^{17}	7×10^{16}	140	Good
S3	W 1.9×10^{-8}	1.3×10^{-4}	4×10^{18}	3.5×10^{18}	65	Bad
S4	W 5.4×10^{-9}	1.3×10^{-4}	10^{18}	2×10^{18}	110	Badly pitted
S5	A 1.8×10^{-10}	1.0×10^{-4}	4×10^{16}	10^{17}	140	Very good
S6	A 6.7×10^{-10}	1.0×10^{-4}	1.4×10^{17}	10^{17}	135	Very good
S7	A 1.8×10^{-9}	1.0×10^{-4}	4×10^{17}			Good
S8	A 6.6×10^{-10}	1.0×10^{-4}	1.4×10^{17}	2×10^{18}	80	Badly pitted
S9	Undoped	1.0×10^{-4}	---			Seed improperly located
S10	Undoped	1.0×10^{-4}	---	9×10^{4} ohm - cm		Seed improperly located
S11	A 6.7×10^{-10}	1.0×10^{-4}	1.4×10^{17}	6×10^{16}	120	Good
S12	Undoped	1.0×10^{-4}	---	590 ohm - cm		Good
S13	A 1.8×10^{-10}	1.0×10^{-4}	4×10^{16}			Thin, seed too hot, 815 °C
S14	A 9.2×10^{-10}	1.0×10^{-4}	2×10^{17}			Good, 807 °C
S15	A 9.2×10^{-10}	1.0×10^{-4}	2×10^{17}	5×10^{17}	90	Good
S16	A 9.2×10^{-10}	1.0×10^{-4}	2×10^{17}			Average
S17	Undoped	1.0×10^{-4}	---			Good
S18	A 9.2×10^{-10}	1.0×10^{-4}	2×10^{17}			Average to poor
S19	M 9.5×10^{-10}	1.0×10^{-4}	2×10^{17}			Average
S20	A 9.2×10^{-10}	1.0×10^{-4}	2×10^{17}			Average
S21	Undoped	1.0×10^{-4}	---	2.5×10^{4}	75	Good
Zn1	Zn:Ga = 2:107	1.0×10^{-4}	1.3×10^{17}	3×10^{16}	40	Average

†A - Sulfur at 56.5 °C, vapor pressure 4.4×10^{-4} mm Hg.
M - Sulfur at 64.7 °C, vapor pressure 8.9×10^{-4} mm Hg.
W - Sulfur at 100 °C, vapor pressure 1.1×10^{-2} mm Hg.

‡Good, average, etc., refer to the appearance of the surface and the thickness of the grown crystal. Very good refers to an approximately 0.8-mm-thick crystal with smooth surfaces. Bad refers to a thin or wedge-shaped crystal with rough surfaces.

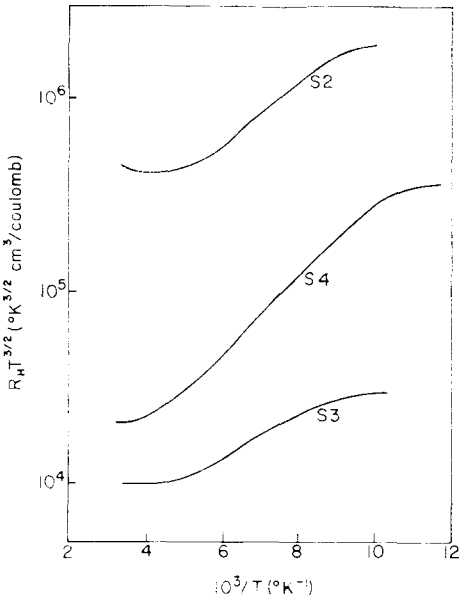

FIG. 6. THE HALL COEFFICIENT TIMES $T^{3/2}$ VS $10^3/T$ FOR THREE DIFFERENT SULFUR-DOPED GaP CRYSTALS.

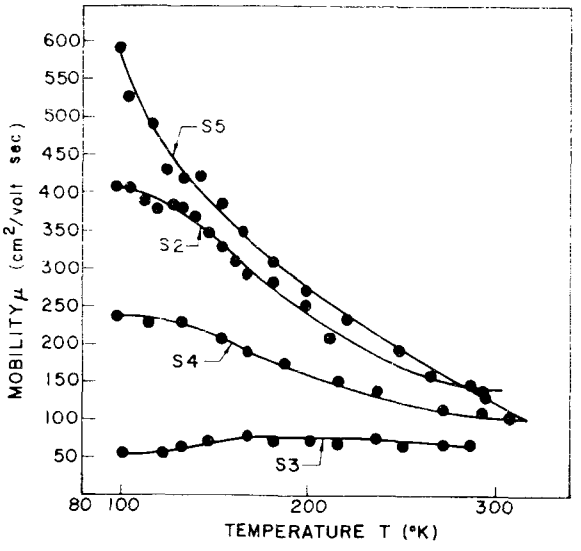

FIG. 7. HALL MOBILITY OF ELECTRONS FOR FOUR DIFFERENT SAMPLES OF SULFUR-DOPED GaP.

The electrical data for the zinc-doped crystal are given in Fig. 8. The Zn ionization energy of 0.032 eV deduced from the data is in good agreement with the value estimated by Madelung [Ref. 14]. Finally, the data from an undoped crystal (S21) are given in Fig. 9; these data suggest that the sample contains about 10^{14} cm^{-3} shallow donors and possibly a larger concentration of other impurities.

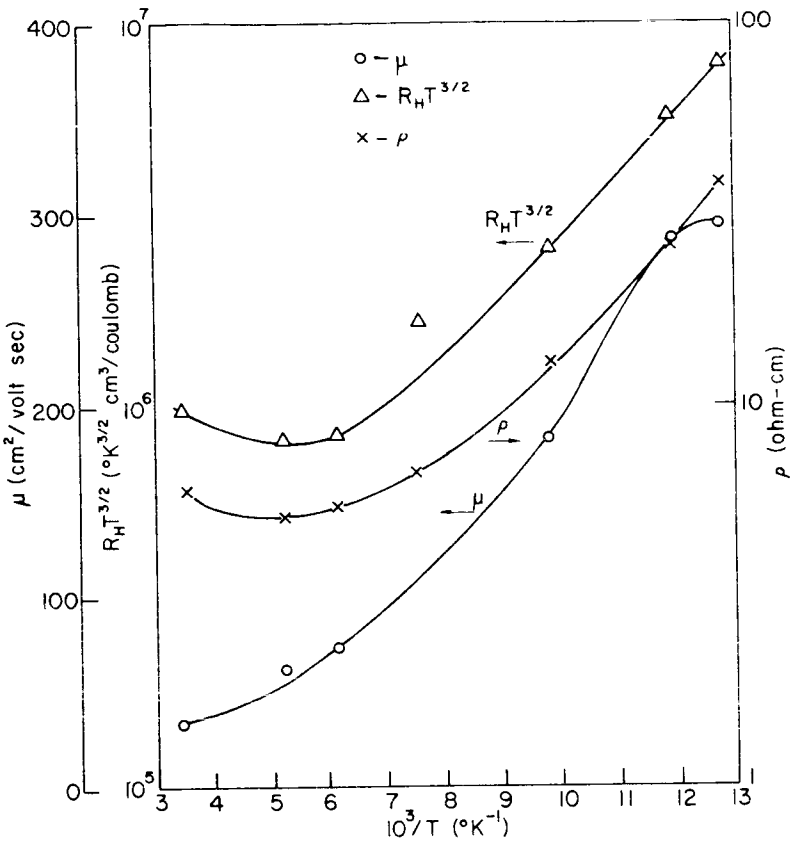

FIG. 8. ELECTRICAL PROPERTIES OF ZINC-DOPED GaP (Zn1).

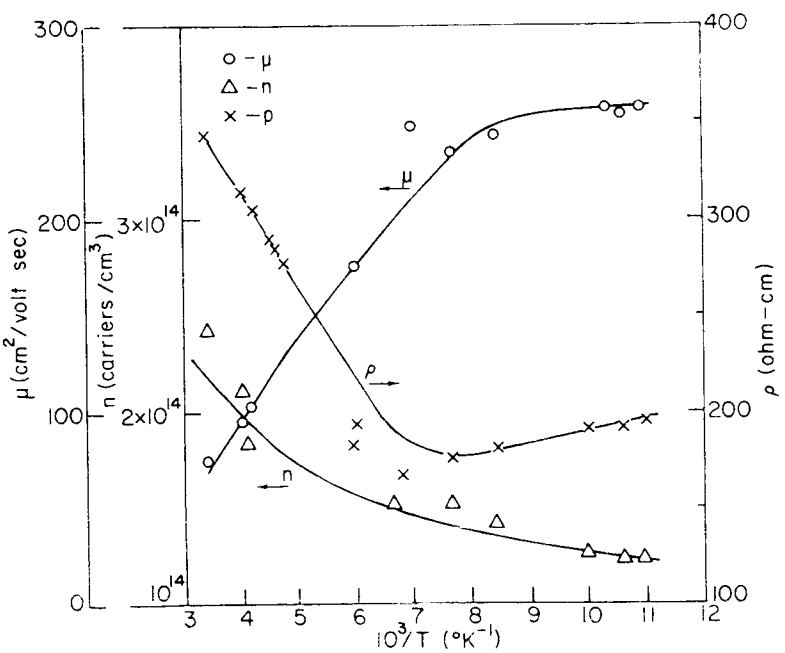

FIG. 9. ELECTRICAL PROPERTIES OF UNDOPED GaP (S21).

1. Effects of Temperature Gradient at the Substrate

Trial and error showed that undoped crystals had to be grown at 815 to 818 °C and that the temperature had to be lowered to 805 to 807 °C to grow crystals doped in the high 10^{17} cm^{-3} range and above. Since the temperature range from 817 to 805 °C corresponded to only 0.6 cm in the 20 °C/cm temperature gradient of the furnace, the seed had to be carefully positioned. If the seed was properly positioned, a crystal with nearly parallel faces could be grown in spite of the temperature gradient. Under good growth conditions, the thickness of the crystal did not vary by more than 100 microns across the growth face. Apparently, at the right location the combination of boat shape and temperature gradient was such that the depletion of the gas stream at the low-temperature edge of the substrate was closely compensated by the increase in the driving force for growth due to the lower temperature.

2. Control of Doping

As shown in Table 4, the electron concentration at room temperature was usually within a factor of 2 of the expected doping. There was no apparent correlation between the conditions of growth and the agreement between the calculated and the observed electron concentrations. Since very little is known about the doping process, predicting the doping to within a factor of 2 is quite satisfactory. The sulfur did not seem to interfere with the growth, except of course that it was observed that heavily sulfur-doped crystals had to be grown at lower temperatures than undoped ones. The growth rates for both sulfur-doped and undoped crystals were always between 1 and 1.5 microns/min when the seed was properly located.

3. Ionization Energy of Sulfur

The purpose of the following discussion is to show that there are unexplained wide variations in the experimentally measured ionization energy of sulfur donors. The ionization energy of sulfur may be important in the design of GaP devices for use over a wide temperature range.

Values for the sulfur ionization energy E_S can be calculated from the plots in Fig. 5 if it is assumed that sulfur is the dominant

impurity. The slopes of the straight lines that make up the low-temperature parts of the plots should yield either E_S or $E_S/2$, depending on whether or not the crystals contain an acceptor impurity that partially compensates the sulfur [Ref. 15]. The slopes, converted to millielectron volts through the use of the formula

$$n = n_o \exp\left(\frac{E}{kT}\right) , \tag{3.1}$$

are listed in Table 5. Notice that the largest value given in the table is three times the smallest value rather than twice the smallest as the theory predicts. No correlation exists between the electron concentrations and the calculated energies.

TABLE 5. VALUES USED TO ESTIMATE THE SULFUR IONIZATION ENERGY

Sample	Electron Concentration (at 300 °K) (electrons/cm^3)	Slope from Fig. 5 (meV)
S1	5×10^{17}	40 ± 1
S5	10^{17}	41 ± 1
S6	10^{17}	24 ± 1
S8	2×10^{18}	64 ± 1
S11	6×10^{16}	72 ± 1

In order to emphasize the spread in the available data on the sulfur ionization energy, the data in Table 5 and those of Montgomery and Feldman [Ref. 16] are plotted in Fig. 10. The values from Table 5 were multiplied by 2 whenever this brought them into closer agreement with the published values. The multiplication was done to emphasize the fact that the measured values for the sulfur ionization energy appear widely spread even if the data shown in Table 5 are adjusted. The results from 15 samples are shown in Fig. 10. The data points spread from 0.048 to 0.103 eV, with an average value of about 0.08 eV.

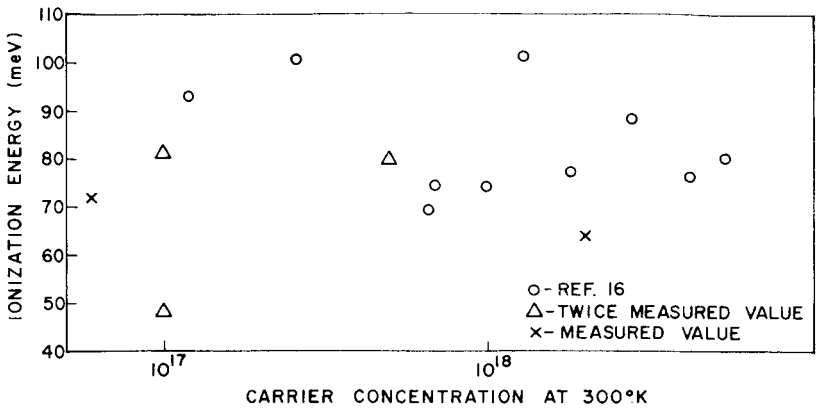

FIG. 10. SULFUR IONIZATION ENERGY VS CARRIER CONCENTRATION.

D. SUMMARY

Both n- and p-type GaP crystals used in this study were produced in an open-tube epitaxial growth system. An accurate determination of the ionization energy of sulfur is suggested as a subject for future research.

IV. RADIOTRACER DIFFUSION

This chapter is concerned with the diffusion of cobalt into GaP and the method used to prepare the samples for Hall effect and optical experiments.

A. EXPERIMENTAL PROCEDURES

Cobalt-60, which has a half-life of 5.2 years, was used as the radiotracer in these experiments. Counting was done in a β-ray proportional counter.

1. Processing of Cobalt-60

A layer of cobalt, vacuum evaporated onto GaP wafers, provided the diffusion source. The cobalt was put directly on the wafers because its vapor pressure is too low at all temperatures below the melting point of GaP to permit the use of gas phase diffusion techniques. The cobalt was evaporated from thin layers of the metal which had been electroplated on tantalum filaments. The cobalt-60 for the electroplating bath was purchased from New England Nuclear Corporation[†] in the form of a mixture of radioactive and elemental cobalt dissolved in HCl. The specifications of the solution as received were as follows:

Specific activity	319 curies/gm
Co^{60}	2.96×10^{-7} moles
Co^{59}	7.7×10^{-7} moles
HCl	1.4 N
Total activity	20 millicuries
Total volume	2.24 ml

In order to prepare an electroplating bath, it was necessary to add nonradioactive cobalt and potassium hydroxide to the solution. The

[†]New England Nuclear Corp., Boston, Mass.

bath was buffered with boric acid. The composition found most satisfactory for plating was as indicated below:

Co^{60}	1.16×10^{-4} molar
Co^{59}	5.73×10^{-2} molar
K^{+}	1.14 molar
B_2O_3	0.294 molar
ph	$\simeq 5$
Total volume	1.14 ml
Ratio $Co^{59}:Co^{60}$	495:2

The bath was used at 60 °C. A current of 1 ma was used to plate the cobalt on tantalum filaments 0.27 mm in diameter by 1.5 cm long (total area of 0.12 cm^2).

2. Diffusion Procedure

The specimens for diffusion were cut from single-crystal epitaxially grown GaP wafers. They were lapped with 3200 grit abrasive, soaked in warm KCN solution (10% KCN in H_2O),[†] washed in deionized water, and rinsed in alcohol. The fixture shown in Fig. 11 was used to evaporate cobalt onto the wafers. A vacuum of 10^{-6} torr was maintained during the evaporation.

The ampoules used in these experiments had the following characteristics. They were constructed of 4-mm-bore Thermal American or Engelhard Industries suprasil grade quartz.[‡] Suprasil quartz is a very pure form of quartz.[†] The ampoules were vacuum fired immediately before use to drive out any absorbed water vapor. Quartz plugs were used to reduce the volume of the ampoules to as small a value as possible. With the plugs in place, the internal volume of the ampoules was typically about 0.1 cc.

[†]The use of a KCN bath [Ref. 17] and of high purity quartz [Ref. 18] have been suggested as ways of preventing copper contamination.

[‡]Thermal American Fused Quartz Co., Montville, N.J.; Engelhard Industries, Inc., Amersil Quartz Div., Hillside, N.J.

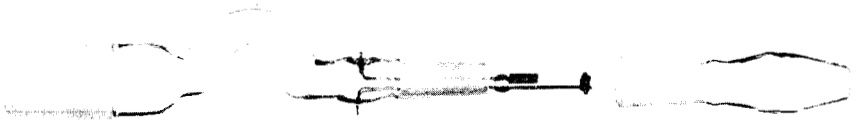

FIG. 11. PHOTOGRAPH OF THE RADIOTRACER EVAPORATION FIXTURE.

Approximately 100 μg of red phosphorus was sealed in the diffusion ampoules along with the sample to prevent the decomposition of GaP and to establish an unambiguous thermodynamic system [Ref. 19]. The pressure inside a 0.1-cc ampoule due to the added phosphorus is shown as a function of the diffusion temperature in Fig. 12. The pressure in any ampoule may have varied by a factor of 2 from the values shown in Fig. 12 due to the difficulties in weighing the phosphorus and in sealing the ampoules.

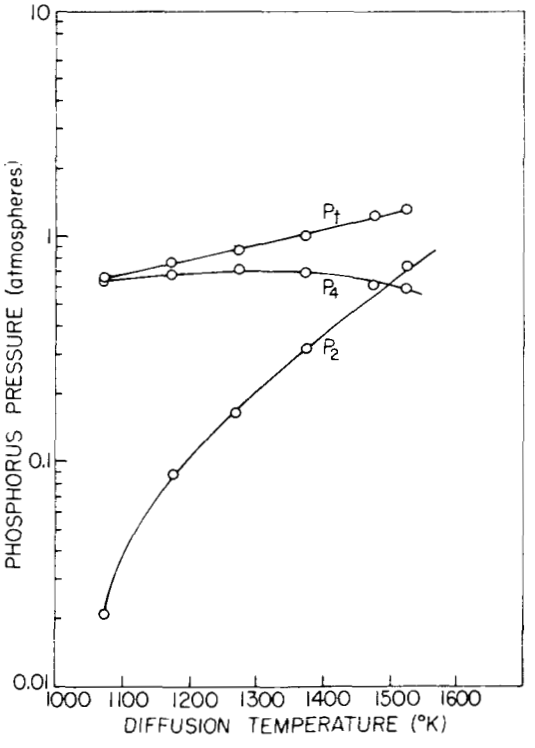

FIG. 12. THE TOTAL PRESSURE AND THE PARTIAL PRESSURES FROM P_2 AND P_4 INSIDE A 0.1-cc AMPOULE CONTAINING 100 μg OF PHOSPHORUS.

Diffusions were performed at temperatures between 900 and 1250 °C for times between 30 minutes and 62 hours. The main problem encountered in the diffusions was that some transport of the sample occurred; the transport agent was probably water vapor from the quartz [Ref. 20]. The vacuum firing of the quartz kept the amount of transport within tolerable limits at temperatures below 1200 °C, but did not prevent it entirely. Above 1250 °C the transport became so severe that no data could be taken.

After diffusion, the crystal was removed from its ampoule and one or more 2.5-mm disks were cut from it with an ultrasonic cutter. One disk was then mounted in a precision lapping machine and layers between 1/2 and 40 microns thick were removed. The amount of material removed was determined by weighing the disk before and after lapping. The cobalt concentration in a lapped layer was determined from a measurement of the beta activity of the alumina plate on which the disk had been lapped.

3. Construction of Diffusion Profiles

The cobalt concentration was calculated from the beta activity of the plate in the following way. Let c be the number of counts per minute measured by the counter, minus the background, when a layer weighing Δw grams had been lapped from the disk. An independent measurement with a cobalt-60 standard showed that the ratio of counts to cobalt-60 decays was 0.17 to 1. The cobalt-60 concentration $[Co^{60}]$ is given by

$$[Co^{60}] = (1.67 \times 10^{7}) \frac{c}{0.17\ \Delta w} \rho_{GaP} . \qquad (4.1)$$

The total cobalt concentration $[Co]$ is given by

$$[Co] = (1.67 \times 10^{7})\ (495) \frac{c}{0.17\ \Delta w} \rho_{GaP} \qquad (4.2)$$

which gives

$$[Co] = \frac{0.87 \times 10^{10}\ c}{\Delta w} . \qquad (4.3)$$

In the expressions above, ρ_{GaP} is the density of GaP (4.13 gm/cc) and the concentrations are in atoms per cc. A straightforward calculation shows that the thickness of the removed layer, in centimeters, is

$$t = 4.92\ \Delta w\ . \qquad (4.4)$$

Diffusion profiles were constructed by inserting measured values of Δw and c into the above formulas.

4. Error Analysis

An estimate of the accidental error in a concentration measurement is given in Fig. 13. The error was taken to be the sum of an error of ±4 percent due to lapping, weighing, etc., and an error due to counting. The latter was calculated as follows. The standard deviation in the number of counts above background σ_C is given by [Ref. 21]

$$\sigma_C = \sqrt{C_T + C_B} \qquad (4.5)$$

where C_T is the total number of counts and C_B is the number of background counts. Equations (4.3) and (4.5) were used to calculate standard deviations in concentration. This was possible because all counting was

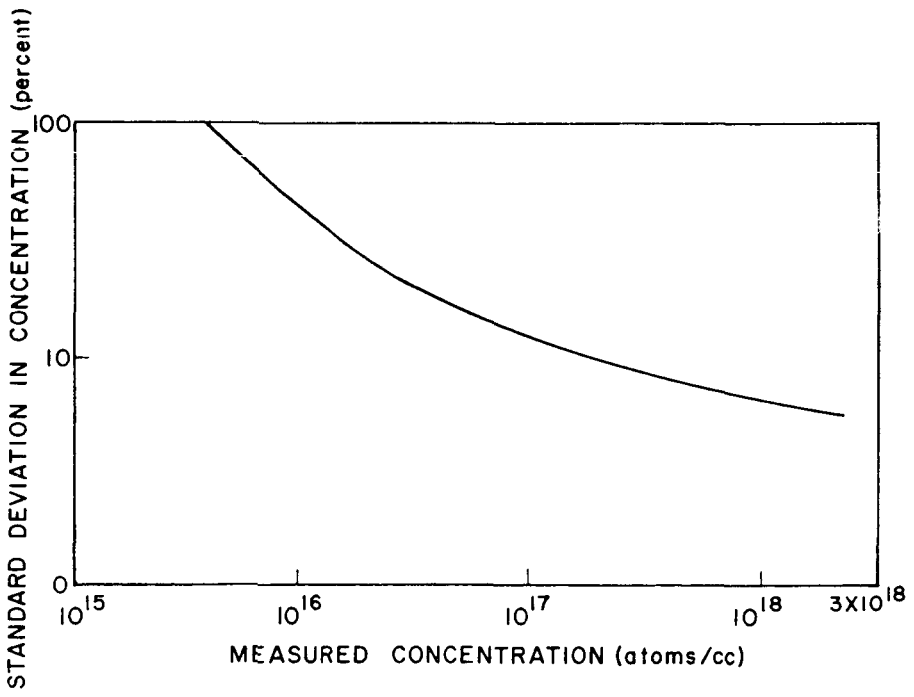

FIG. 13. ESTIMATE OF ACCIDENTAL ERROR IN RADIOTRACER CONCENTRATION MEASUREMENTS.

for 1 minute so that the number of counts per minute and the number of counts were equal. [Eq. (4.3) requires a counting rate; Eq. (4.5) requires a number of counts.] Typical experimental values of 20 counts per minute for the background and of 100 μg for Δw were used in the calculations.

The plot in Fig. 13 shows that the error for concentrations of less than 10^{16} cm^{-3} is very large. This large error is a direct consequence of the fact that nonradioactive cobalt had to be added to the high specific activity solution purchased in order to obtain a solution that would plate satisfactorily. This error is the major drawback resulting from the plating method of preparing the radiotracer.

B. RESULTS OF DIFFUSION

The results of the radiotracer work are presented as plots of the logarithm of the cobalt concentration vs the distance from the crystal face that had been coated with radiotracer cobalt. The error limits have been omitted from some of the figures for the sake of clarity. The error can always be determined by referring to Fig. 13. Since the aim of the radiotracer work was to produce uniformly doped samples, most of the diffusions were done for combinations of time and temperature which promised to give the flattest profiles.

A typical diffusion profile is shown in Fig. 14. It consists of a region of rapidly decreasing concentration near the surface followed by a region in which the cobalt concentration is nearly constant. Similar profiles have been reported for the diffusion of transition and noble metals into GaAs and other III-V compounds [Ref. 22].

Typical results of a series of diffusions for the same time but at different temperatures are shown in Fig. 15. Notice that the cobalt concentration in the central region increases as the diffusion temperature increases. In Figs. 16 and 17, the results of diffusions for different times at the same temperature are shown. Data from two different crystals were included in Fig. 17 only after the data were proved to be consistent.

The data shown in Fig. 18 were taken to determine if the diffusion profiles in p-type crystals were noticeably different from those in n-type crystals. Little difference is noted.

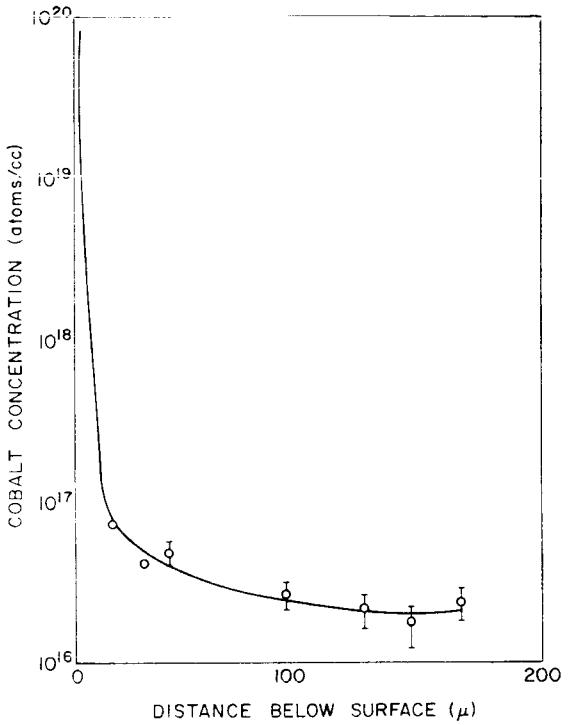

FIG. 14. TYPICAL DIFFUSION PROFILE FOR COBALT IN GaP. Crystal S4 (sulfur $> 2 \times 10^{18}$ cm^{-3}), 29 hr, 1015 °C.

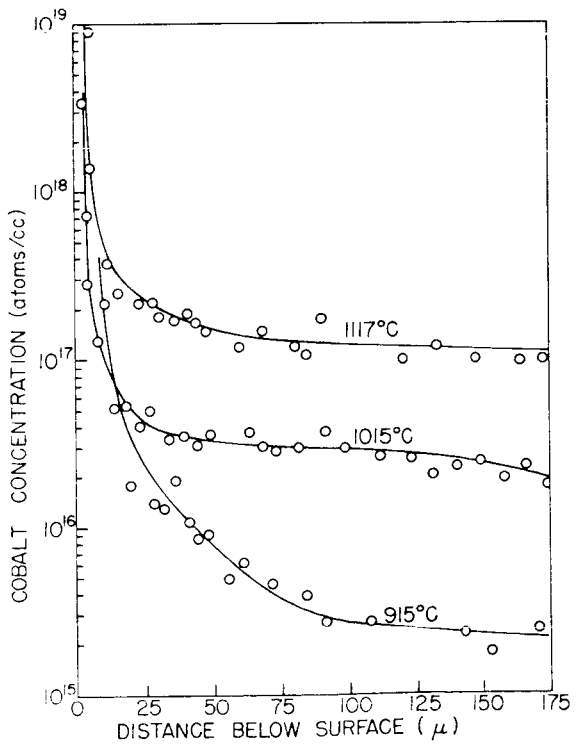

FIG. 15. COBALT PROFILES AFTER 24-HR DIFFUSIONS AT DIFFERENT TEMPERATURES IN GaP. Crystal S4 (sulfur $> 2 \times 10^{18}$ cm^{-3}).

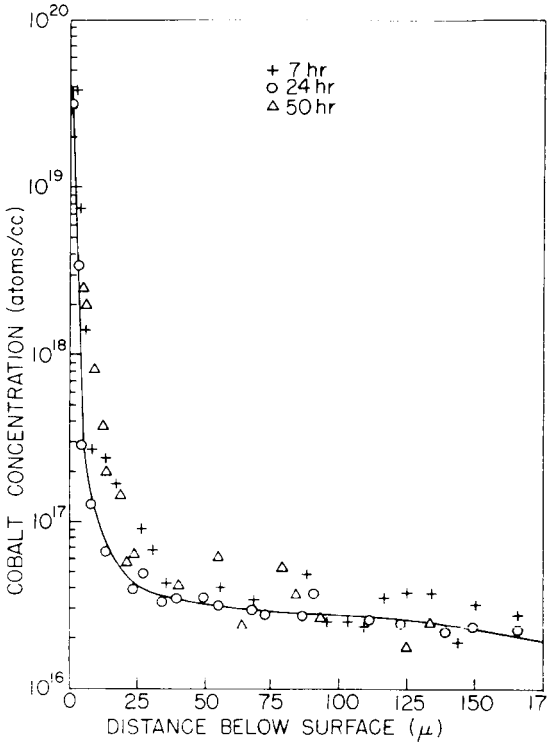

FIG. 16. COBALT PROFILES AFTER DIFFUSION AT 1015 °C FOR DIFFERENT TIMES IN GaP. Crystal S4 (sulfur $> 2 \times 10^{18}$ cm^{-3}).

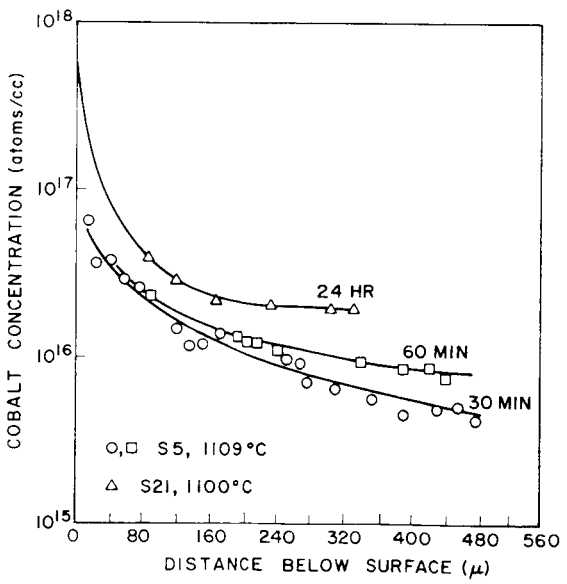

FIG. 17. COBALT PROFILES AFTER DIFFUSIONS AT 1100 °C FOR DIFFERENT TIMES.

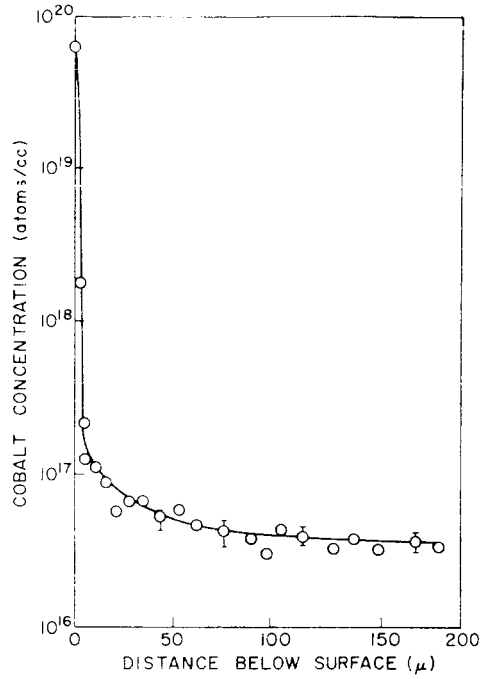

FIG. 18. COBALT PROFILE AFTER 1100 °C DIFFUSION FOR 24 HR IN p-TYPE GaP. Crystal Zn1 ($Zn \simeq 6 \times 10^{18}$ cm^{-3}).

The preliminary diffusion data shown in the figures suggested that the flattest profiles would be obtained by diffusing into a wafer from both faces of the wafer. Typical results of such diffusions are given in Fig. 19. The asymmetry in the profiles is due to crumbling of the samples during lapping.

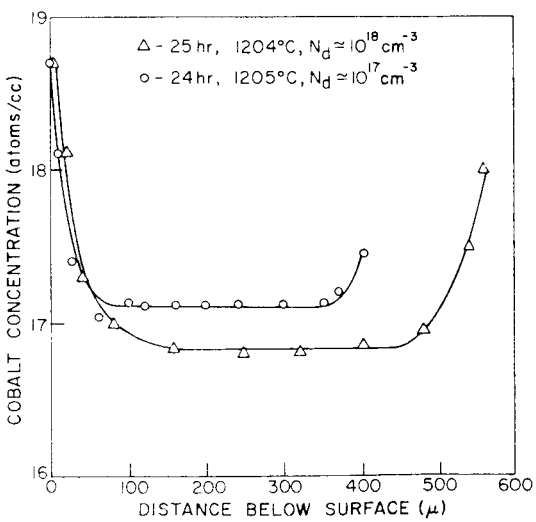

FIG. 19. PROFILES FOR COBALT DIFFUSED FROM BOTH SIDES OF A WAFER.

C. DISCUSSION OF DIFFUSION DATA

1. Preparation of Electrical and Optical Samples

The most important conclusion to be drawn from the data is that uniformly cobalt-doped samples of GaP can be prepared by diffusion. The fact that diffusion leads to a wide region of crystal with a nearly uniform cobalt concentration is particularly evident in Fig. 19. A uniformly doped sample is easily obtained from a diffused sample by lapping off the regions of rapidly decreasing concentration. Also, the concentration attained after a 1200 °C diffusion was large enough to be detected in the Hall effect and optical transmission experiments.

The samples used in the electrical and optical experiments were diffused for 24 hours with cobalt on both sides of the wafer, or for times up to 62 hours with cobalt on only one side. Samples diffused from one side were used before the idea of diffusing from both sides occurred to the author. Both diffusion methods led to identical Hall effect data and optical transmission results.

2. Diffusion Mechanism

The three features of the profiles that are most indicative of the diffusion mechanism are as follows:

1. The shape cannot be described by either a gaussian or an error function curve.
2. The profile does not change significantly after 7 hours of diffusion (Fig. 16).
3. The 30-minute and 1-hour profiles are more rounded than the profiles for long diffusion times (Fig. 17).

These three observations suggest that the profile is the result of two diffusion mechanisms operating simultaneously. In particular, it appears that the steep part of the profiles is due to a substitutional diffusion mechanism that carries a large concentration of cobalt at a very slow rate. The flat part of the profiles must be due to interstitial diffusion. These hypotheses explain the third observation in the following way. After very short diffusions, the interstitial and the substitutional profiles are both rounded and their sum, which is the observed profile, is also rounded. After a long diffusion, the interstitial profile is flat and a corner results where it intersects the substitutional part of the profile.

3. Concentration of Cobalt in GaP

The cobalt concentration obtained from the flat part of a number of profiles is shown in Fig. 20.† The plots in the figure show that the concentration depends on the crystal used for the diffusion, as well as on the diffusion temperature. Some possible explanations are given below.

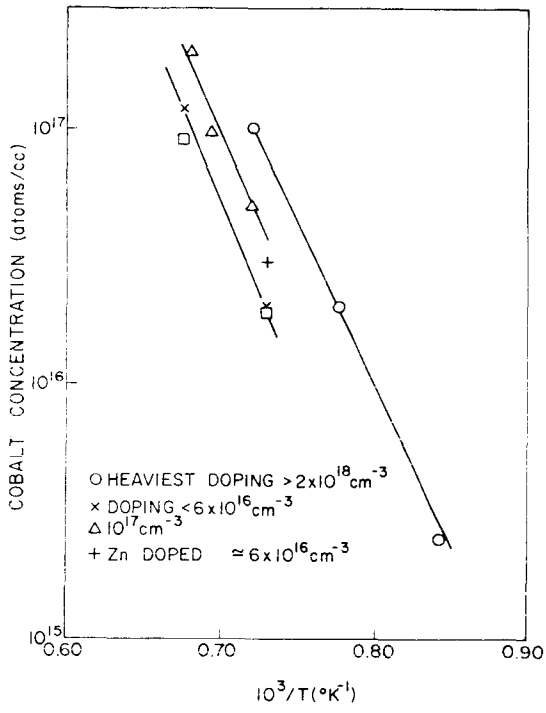

FIG. 20. COBALT CONCENTRATIONS IN THE FLAT PARTS OF THE DIFFUSION PROFILES.

It is reasonable to expect that the cobalt concentration should depend on the time and temperature of diffusion, the phosphorus overpressure, the initial doping of the crystal, and the density of defects in the crystal. Any dependence on time and on overpressure was eliminated by diffusing for more than the 7 hours required by the data in Fig. 16 and by fixing the phosphorus pressure near 1 atmosphere. The temperature dependence shown in Fig. 20 can be described by the formula

$$C = C_o \exp\left(-\frac{1.1}{kT}\right) , \qquad (4.6)$$

† It is important that the data in Fig. 20 be considered as concentrations obtained after diffusion and not as solubilities.

where C is the cobalt concentration. C_o depends on the particular crystal, but the activation energy of 1.1 eV is a constant. The question to be answered is why C_o varies from sample to sample. A comparison of experimental data with calculations based on the Shockley-Moll theory of the effects of doping on solubility [Ref. 23] shows that the changes in C_o cannot be related to the dopings of the crystals. (The comparison is discussed in Appendix A.) Hence it appears that the different values for C_o must have arisen from differences in the defect concentration in the various samples. Unfortunately, the only experimental evidence available to support this hypothesis is that polished pieces taken from the crystals for which C_o was largest appeared less perfect when viewed by transmitted light than did pieces from the other crystals. A qualitative relation between the cobalt concentration and the defect concentration could possibly be obtained from dislocation etch studies and lattice constant measurements [Ref. 24].

D. SUMMARY

Radiotracers have been used as a tool to develop a method of preparing GaP samples that contain a known cobalt concentration. It is concluded that cobalt diffuses both substitutionally and interstitially. The interstitial diffusion gives the long flat part of the diffusion profile. The concentration in the flat part of the profile depends on both the diffusion temperature and the crystal used. The dependence of the cobalt solubility on crystal perfection is suggested as an area for future work.

V. ELECTRICAL MEASUREMENTS

Hall effect and resistivity measurements were used to determine the electrical properties of cobalt-doped GaP. The measurements required the use of special high-resistance measuring equipment.

A. EXPERIMENTAL EQUIPMENT

Preliminary measurements showed that the equipment used to measure the Hall effect and resistivity of the sulfur-doped crystals was not suitable for measurements on cobalt-doped samples. Neither the electrical insulation nor the temperature control nor the shielding were adequate for measurements on high-resistance samples.

Suitable Hall effect equipment was assembled and is shown in Figs. 21 through 24. A Keithley[†] electrometer (Model 610 BR) was used to measure the resistivity and Hall voltages. A microvolt-ammeter with full-scale ranges from 10 picoamperes to 100 milliamperes was used to measure the sample current. The current source, nulling source, and all of the switching equipment were mounted on a plexiglass chassis which was enclosed in a well-shielded box. As much as possible of the wiring was insulated with Teflon. The connectors were chosen for their high leakage resistance. The leakage resistance of the complete assembly, including connectors and cabling, was greater than 10^{13} ohms.

The method of temperature control, based on the principle of balancing the heat loss from the sample block with heat supplied by a nichrome heater, permitted measurements at temperatures from 77 to 420 °K. The upper limit was set by the softening temperature of the epoxy used to hold the heater in place. The rate of temperature change at any specified temperature was about 2 deg per 10 minutes. The main experimental problem associated with the temperature control was sealing the outer can in place (see Fig. 23). The most effective method of sealing was to solder the can in place with a low-melting temperature solder such as Cerro-Bend.[‡] However, even this method usually required a number of tries before an adequate vacuum seal was obtained.

[†] Keithley Instruments, Inc., Cleveland, Ohio.

[‡] Cerro-Bend, c/o Peck Louis Corp., Los Angeles, California.

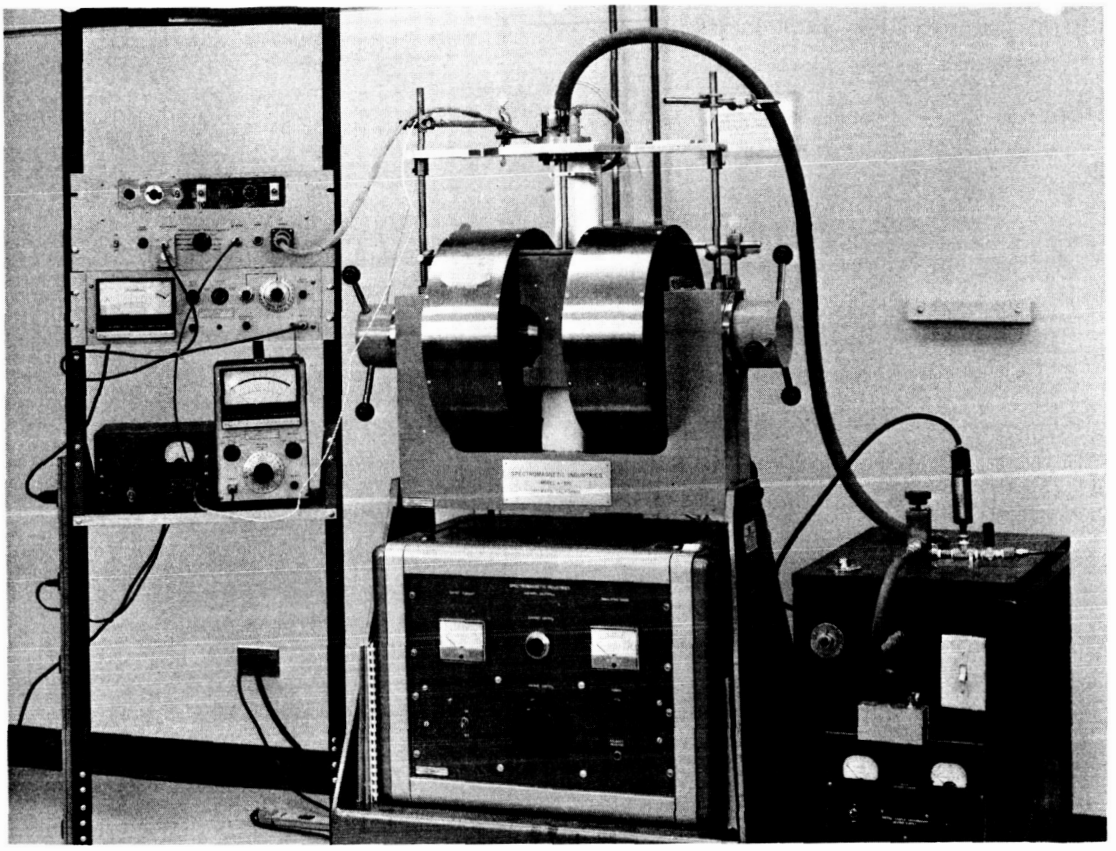

FIG. 21. THE HALL EFFECT APPARATUS USED TO MEASURE HIGH-RESISTANCE SAMPLES.

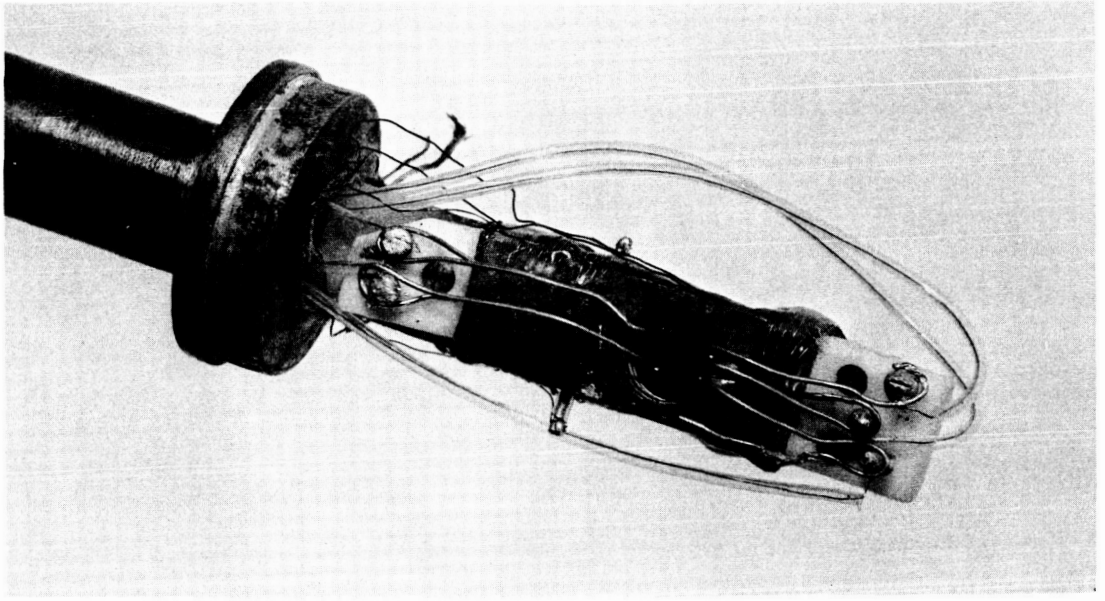

FIG. 22. DETAILS OF THE SAMPLE MOUNT USED FOR HIGH-RESISTANCE SAMPLES.

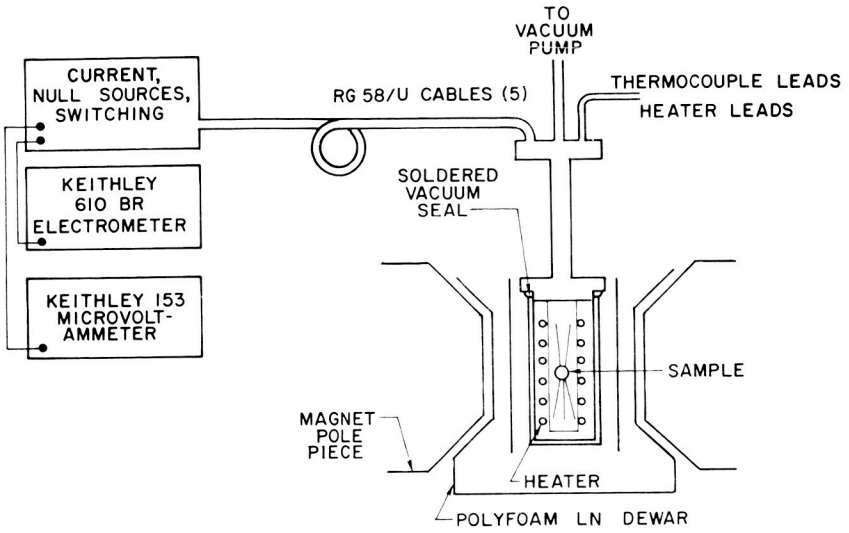

FIG. 23. SCHEMATIC DIAGRAM OF THE HALL EFFECT APPARATUS.

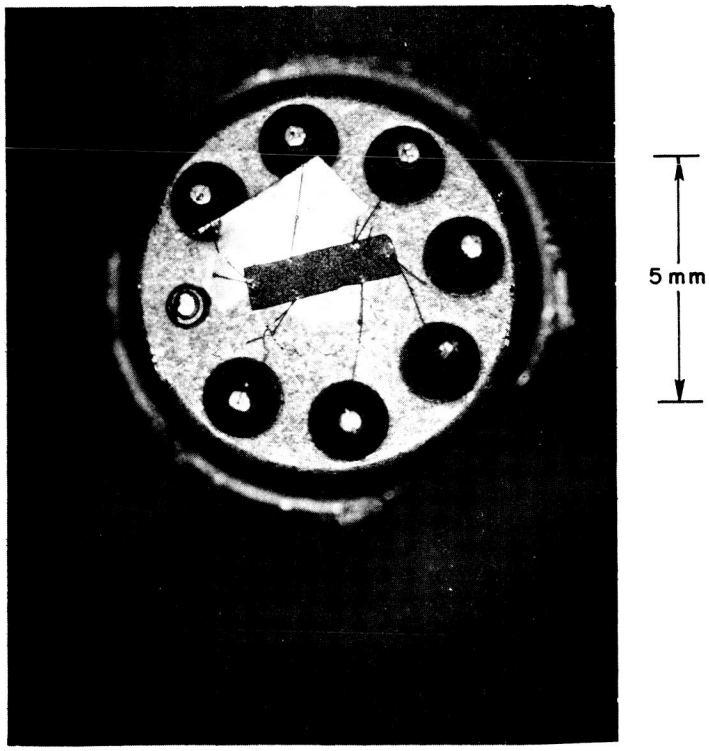

FIG. 24. TYPICAL HALL BAR MOUNTED ON A TO-5 HEADER.

The test samples were bars approximately 3 by 1 by 0.5 mm mounted on TO-5 transistor headers. The bars were prepared by first lapping at least 60 microns off each face of a diffused specimen. Next, gold-2% zinc contacts were evaporated and then alloyed onto the bars. Finally, the bars were temporarily mounted on the headers and six 1-mil wires were bonded to the alloyed contacts. The primary reasons for bonding the wires to the samples were that the bonding process is intrinsically clean and that the available bonding equipment was well suited to handling small delicate samples. When the bonding was complete, the bars were lifted from headers and suspended on the 1-mil wires. This last step was performed so that the bar could not be shorted out by contact with the surface of the header. The finished samples were quite sturdy and could be easily handled.

The use of the transistor headers was the major compromise in the equipment. In order to use the bonding equipment it was necessary to use the headers. Also, the headers make a very satisfactory high-resistance mount. The disadvantage of headers is that they contain kovar which is ferromagnetic. Measurements in the magnet used for the Hall effect work showed that the presence of the header distorted the field enough to cause about a 10-percent increase in the field at the sample. This increase in the magnetic field meant that the measured Hall coefficient had to be multiplied by some factor to obtain the correct Hall coefficient. Since this factor could not be determined accurately, the Hall effect data obtained using the headers were in error. However, because the necessary correction was multiplicative, the increase in the field did not affect any result that depended on the ratio of two Hall coefficients. Since the cobalt ionization energy is calculated from the ratio of Hall coefficients (see Section V.D1), the headers did not seriously interfere with the main purpose of the measurement.

B. RESULTS OF HALL AND RESISTIVITY MEASUREMENTS

The results of a number of Hall effect and resistivity measurements on cobalt-doped GaP are summarized in Fig. 25. The data points are from two samples, each of which contained 6×10^{16} cm^{-3} sulfur and 9×10^{16} cm^{-3} cobalt atoms. Hall measurements made on a number of samples with various

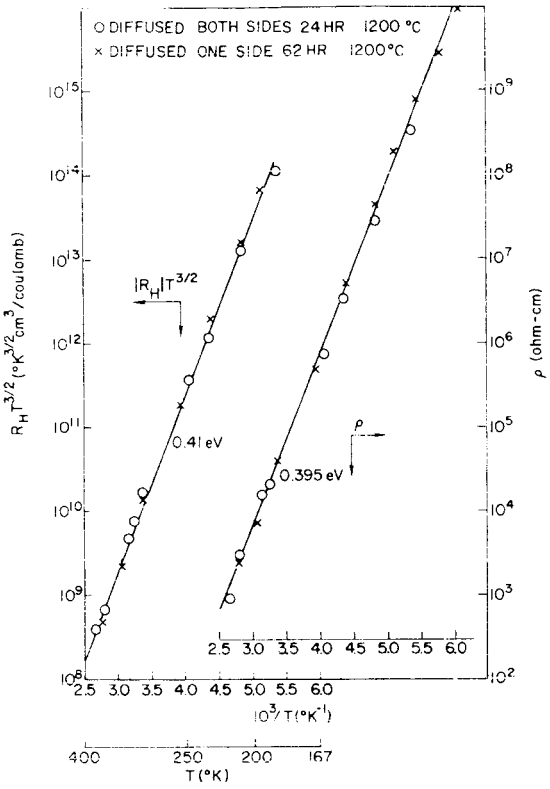

FIG. 25. HALL COEFFICIENT AND RESISTIVITY DATA FOR COBALT-DOPED GaP. Samples 1 and 2 are designated by X and O, respectively.

combinations of cobalt and sulfur dopings showed that the data in Fig. 25 could be attributed to a cobalt impurity level. The sign of the Hall coefficient showed that cobalt acts as an acceptor.

Hall mobility calculated from the data in Fig. 25 is shown in Fig. 26. As expected, the values are somewhat less than those reported by Allen [Ref. 25] for less heavily compensated GaP.

C. COBALT IONIZATION ENERGY

The cobalt ionization energy is calculated from the Hall effect data through the use of Fermi statistics and the principle of charge neutrality. The first step in this calculation is to relate the slope of the plots in Fig. 25 to the location of the Fermi level. This step is accomplished in the following way. The concentration of holes p is related to the Hall coefficient by the approximate relation

$$p = \frac{1}{(R_H q)} , \qquad (5.1)$$

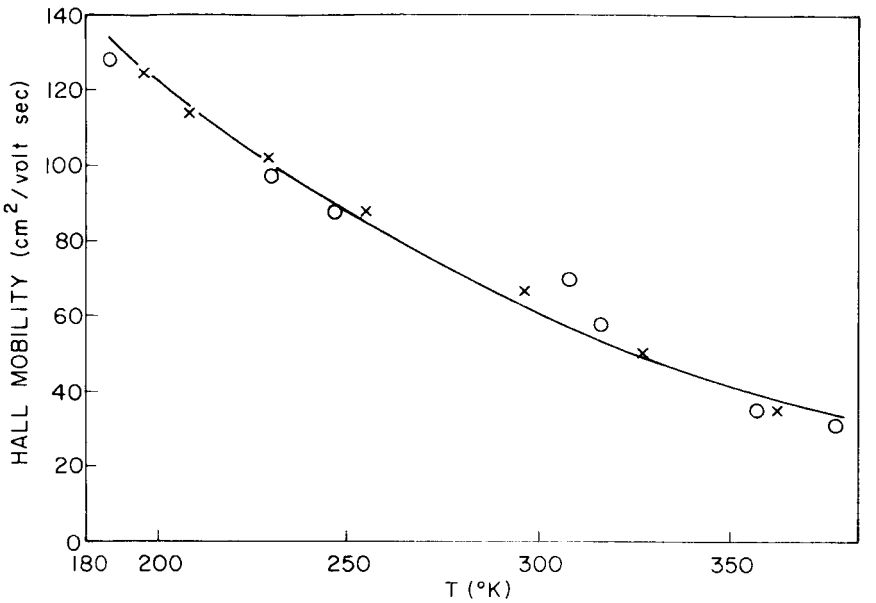

FIG. 26. HALL MOBILITY OF HOLES IN COBALT-DOPED GaP. Samples 1 and 2 are designated by X and O, respectively.

where q is the electronic charge. The concentration of holes is also given by

$$p = N_V \exp\left(-\frac{E_F}{kT}\right), \tag{5.2}$$

where N_V is the density of states in the valence band and E_F is the Fermi energy measured from the valence band. When N_V, which contains the factor $T^{3/2}$, is written as

$$N_V = N_V' T^{3/2}, \tag{5.3}$$

Eq. (5.2) becomes

$$p = N_V' T^{3/2} \exp\left(-\frac{E_F}{kT}\right). \tag{5.4}$$

Equivalently,

$$pT^{-3/2} = N_V \exp\left(-\frac{E_F}{kT}\right), \tag{5.5}$$

where the only temperature-dependent term on the right side is the exponential. Together Eqs. (5.1) and (5.5) yield

$$R_H T^{3/2} = C \exp\left(\frac{E_F}{kT}\right), \tag{5.6}$$

where all of the temperature-independent terms have been combined into C. Taking logarithms gives

$$\ln\left(R_H T^{3/2}\right) = \ln C + \frac{E_F}{kT} . \tag{5.7}$$

After differentiation with respect to 1/T, Eq. (5.7) becomes

$$\frac{d\left(\ln\left(R_H T^{3/2}\right)\right)}{d(1/T)} = \frac{E_F}{k} - \frac{T}{k}\frac{d}{dT} E_F . \tag{5.8}$$

For the case in which the slope of a plot of $\ln\left(R_H T^{3/2}\right)$ vs 1/T is a constant, Eq. (5.8) may be simplified to

$$\frac{E_F}{k} - \frac{T}{d}\frac{d}{dT}\left(E_F\right) = \text{constant} . \tag{5.9}$$

The differential equation yields

$$E_F = E_F^o + \beta T , \tag{5.10}$$

where E_F^o is the Fermi energy at T = 0 °K and β is the coefficient of temperature variation. In other words, Eq. (5.10) states that if a plot of $\ln\left(R_H T^{3/2}\right)$ vs 1/T is a straight line, the slope of the line gives the value of the Fermi level extrapolated to T = 0 °K. The value of β is determined from the values of R_H at temperatures above 0 °K; however, experimental error frequently makes the determination impossible.

The value of E_F^o deduced from Fig. 25 is 0.41 eV. The value of β cannot be determined from the data; to show this, let us try to calculate β from the 300 °K Hall data. From Fig. 25 the hole density at 300 °K is about 2×10^{12} cm^{-3}. The value of E_F calculated from Eq. (5.2) for $p = 2 \times 10^{12}$ cm^{-3} and

$$N_V = 10^{19} \pm 2 \times 10^{18} \text{ cm}^{-3} \qquad (5.11)^{\dagger}$$

is

$$E_F = 0.40 \text{ eV} \pm 20 \text{ meV} . \qquad (5.12)$$

Hence, the value of β is

$$\beta = 0.41 \text{ eV} - (0.40 \text{ eV} \pm 20 \text{ meV})$$
$$= 10 \text{ meV} \pm 20 \text{ meV} . \qquad (5.13)$$

Clearly, β is lost in the uncertainty in the value of N_V. Notice that the calculation does show that β is small and hence that E_F is nearly equal to E_F^o.

Because of the chemical doping of the samples whose data are shown in Fig. 25, the Fermi energy of 0.41 eV is very close to the ionization energy of cobalt. The exact relation is calculated using the principle of charge neutrality, which requires that

$$p + N_d^+ = N_A^- + n . \qquad (5.14)$$

In Eq. (5.14), p and n are, respectively, the concentrations of holes and electrons, N_d^+ is the concentration of positive donors, and N_A^- is the concentration of negatively charged acceptors. Since in p-type GaP,

$$n \ll p \qquad \text{and} \qquad N_d^+ = N_d , \qquad (5.15)$$

---

†These values of N_V were calculated for hole effective masses of 0.5 to 0.7 times the free electron mass.

Eq. (5.15) may be simplified to

$$p = N_A^- - N_d \quad , \tag{5.16}$$

where N_d is the total donor concentration. When the cobalt and sulfur concentrations are inserted, Eq. (5.16) becomes

$$p = 9 \times 10^{16} \, f - 6 \times 10^{16} \quad , \tag{5.17}$$

where

$$f = \left[\exp\left(\frac{E_A' - E_F}{kT} \right) + 1 \right]^{-1} \tag{5.18}$$

and

$$E_A' = E_A + kT \ln \gamma \quad . \tag{5.19}$$

The quantities E_A and γ are, respectively, the ionization energy and the degeneracy factor of the cobalt level. With the Fermi level at 0.41 eV, p is much less than 6×10^{16} cm^{-3} and hence makes a negligible contribution to the concentration of positive charges. When p is neglected, Eq. (5.17) becomes

$$9 \times 10^{16} \, f = 6 \times 10^{16} \quad . \tag{5.20}$$

The solution to this equation is

$$E_A' = 0.41 \text{ eV} - 0.6 \text{ kT} \quad , \tag{5.21}$$

or, to within the accuracy of the data,

$$E_A' = 0.41 \text{ eV} \quad . \tag{5.22}$$

The quantity E_A cannot be determined until γ is known. However, $\ln \gamma$ is likely to be in the range $-1 < \ln \gamma < 1$ so E_A should be within kT of E_A'.

VI. OPTICAL TRANSMISSION

Optical transmission measurements were performed to determine the d-shell structure of cobalt impurities in GaP. Both n-type and p-type GaP were studied.

A. EXPERIMENTAL EQUIPMENT

Optical transmission measurements were made at 77 °K and 300 °K in a Cary[†] model 14IR recording spectrophotometer at wavelengths between 0.5μ and 3.0μ. The samples were either thin single crystals or thick polycrystals[‡] of GaP containing cobalt. The single-crystal specimens were pieces of epitaxial GaP approximately 3 mm by 2 mm by 0.5 mm. The optical path was either through the 3 mm by 2 mm faces (0.5-mm path length) or through the 3 mm by 0.5 mm faces (path length of 2 mm). The latter orientation was used whenever a long optical path was needed. The single-crystal samples were diffused at 1200 °C.

B. RESULTS OF OPTICAL MEASUREMENTS

Two distinct types of spectra were seen. The first occurred in crystals in which the Fermi level was at or above the 0.41-eV cobalt level. The second was seen in crystals whose Fermi levels were below the cobalt level.

The spectrum shown in Fig. 27 is typical of those measured on samples in which the cobalt acceptors were ionized. The features of the spectrum indicative of the d-shell structure are the decreases in transmission around 0.8μ and between 1.15μ and 1.3μ. The decreases in transmission are more evident in the spectrum of a thick piece of polycrystalline material as shown in Fig. 28.

In Fig. 29 the enhanced absorptions in the 0.8μ and 1.2μ regions are shown separated from the background. The spectrum in this figure is the result of averaging a number of plots like the one shown in Fig. 27. The absorptions shown in Fig. 29 were separated from the background in the

---

[†]Cary Instruments, Applied Physics Corp., Monrovia, California.

[‡]The polycrystalline samples were provided by J. W. Allen.

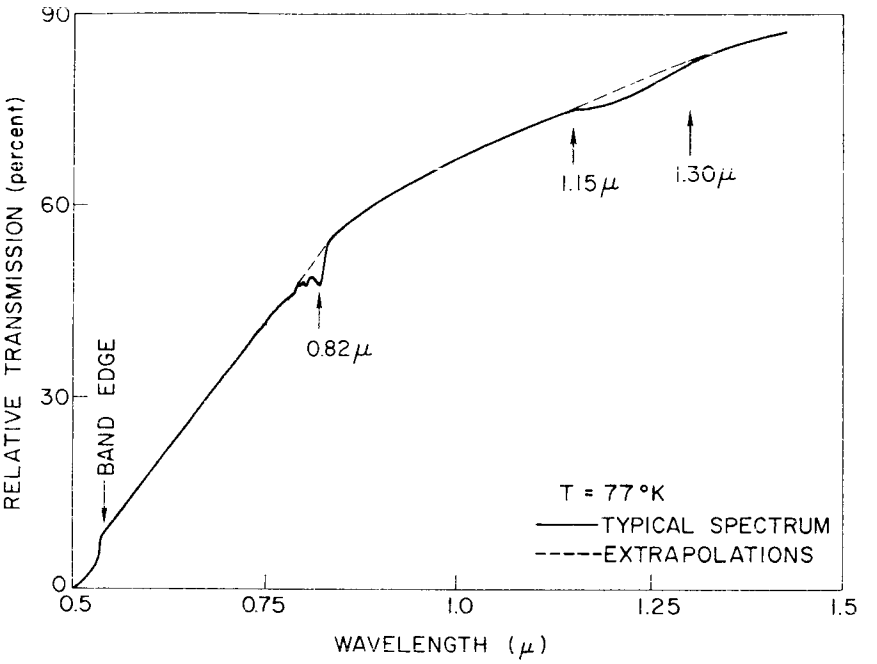

FIG. 27. OPTICAL TRANSMISSION IN ARBITRARY UNITS VS WAVELENGTH FOR n-TYPE SINGLE-CRYSTAL GaP CONTAINING $\simeq 10^{17}$ cm^{-3} COBALT ATOMS.

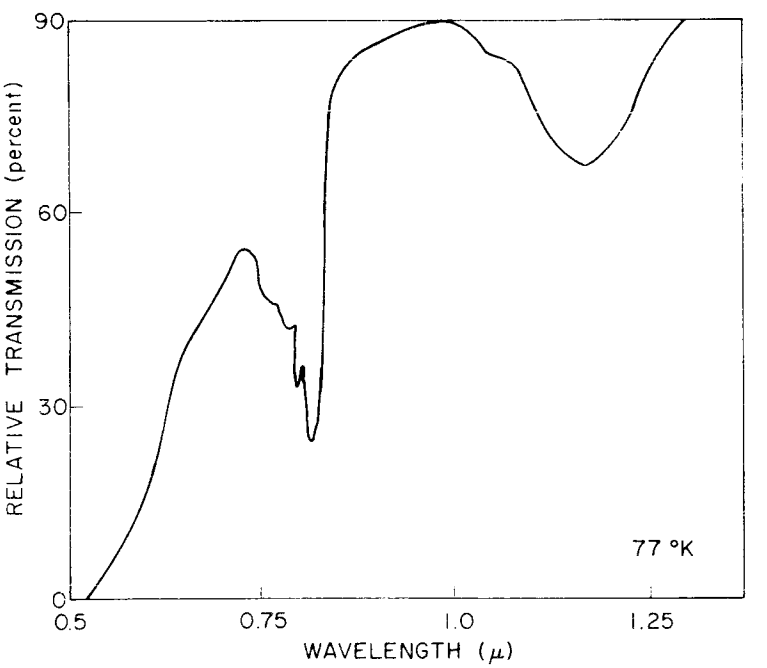

FIG. 28. OPTICAL TRANSMISSION IN ARBITRARY UNITS VS WAVELENGTH FOR n-TYPE POLYCRYSTALLINE GaP CONTAINING COBALT. T = 77 °K.

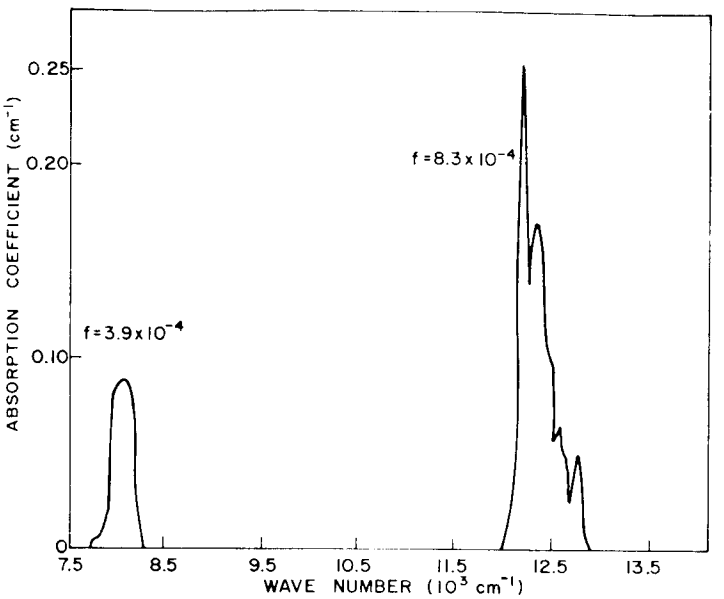

FIG. 29. ABSORPTION AFTER BACKGROUND HAS BEEN SUBTRACTED VS WAVE NUMBER FOR COBALT-DOPED GaP WAFERS. Average values obtained from several samples are shown.

following way. The transmission curves were extrapolated by eye into the 0.8μ and 1.25μ regions as indicated in Fig. 27. An absorption spectrum was calculated from the ratios of actual transmissions to the extrapolated transmissions. The method automatically corrects for reflection and for sample geometry. This method was used because it was the only experimentally feasible technique and because the location of the absorption peaks was more important than the exact shape of the spectrum. The alternative method of eliminating background with the use of a sample of GaP in the reference beam of the spectrometer was not used because the broad features as well as the structure of the spectrum of cobalt-doped GaP depend on the presence of the cobalt.

A typical spectrum of low-resistance p-type samples containing both zinc and cobalt is shown in Fig. 30. The spectrum of the zinc-doped crystal (Zn1 of Chapter III) without cobalt is included for reference. The spectra were extended to 6μ with an infrared spectrometer. These spectra are discussed in Section C.2.

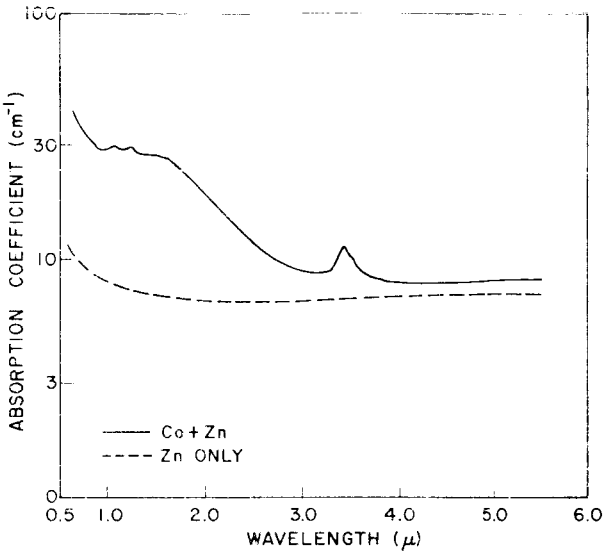

FIG. 30. ABSORPTION SPECTRA OF A GaP WAFER CONTAINING ZINC PLUS $\simeq 2 \times 10^{17}$ cm^{-3} COBALT ATOMS, AND OF A WAFER CONTAINING ONLY ZINC. Zero is arbitrary. T = 300 °K.

C. DISCUSSION OF THE OPTICAL DATA

GaP crystallizes in the zinc blende structure. Since both the substitutional sites and the interstitial sites in that structure have tetrahedral symmetry, the diffused cobalt impurities were on sites with tetrahedral symmetry. The group theoretic properties of the tetrahedral group were given in Tables 1, 2, and 3 of Chapter II. In the following section, d^n is used as shorthand for "d^n configuration with all other shells closed."

1. Filled Cobalt Levels

The absorptions shown in Fig. 29 can be fitted to the crystal field levels of a d^7 ion at the center of a tetrahedron of negative charges. The values of the oscillator strengths are in the range reported for cobalt on tetrahedral sites [Ref. 2]. The spectrum given in Fig. 29 is similar to that reported for d^7 cobalt in ZnS [Ref. 2].

The theoretical spectrum of d^7 in a tetrahedral field was discussed in Chapter II, Section C2. The essential points of that discussion are repeated below. The ground state of a d^7 ion in free space with all shells except the d shell closed is a ^4F configuration. In a tetrahedral field ^4F splits into

$$^4F \rightarrow \left| \begin{matrix} ^4T_1 \\ ^4T_2 \\ ^4A_2 \end{matrix} \right. ,$$

where $^4A_2$ is the ground state of the split levels. The only other quartet level in the eigenvalue scheme for d^7 is a ^4P level which is not split by the crystal field; i.e.,

$$^4P \rightarrow {}^4T_1 .$$

The spin and symmetry allowed transitions are from the $^4A_2$ ground state to the $^4T_1(^4F)$ level and to the $^4T_1(^4P)$ level. The fit of the absorptions shown in Fig. 29 to these two levels is shown in Fig. 31. Two parameters, Dq/B and B, are used in the calculations. The best fit is for $1.8 \leq Dq/B \leq 2.1$ and $275 \leq B \leq 305$ cm^{-1}.

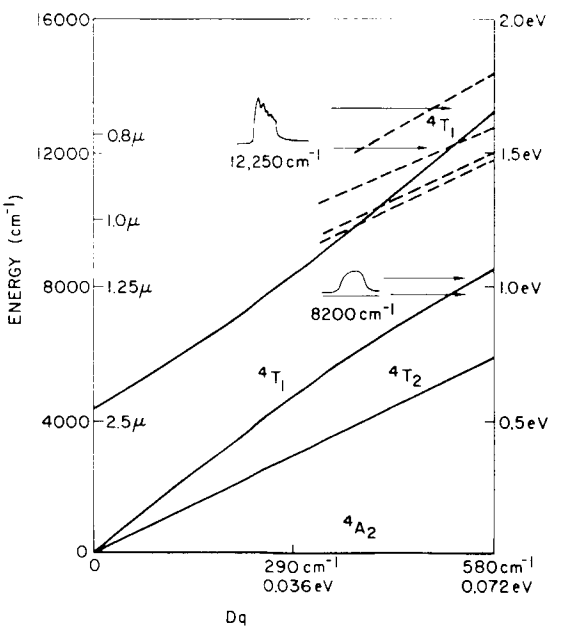

FIG. 31. THE QUARTET TETRAHEDRAL FIELD LEVELS ARISING FROM $3d^7$ AND THE FIT OF THE OBSERVED SPECTRUM TO THEM. Dashed lines indicate approximate positions of some doublet levels.

Some of the structure on the absorption centered at 12,250 cm^{-1} is probably due to spin-orbit mixing of the $^4T_1(^4P)$ level with doublet levels. The approximate positions of some of the doublets are shown on Fig. 31. The precise locations of the doublets depend on the value of the

Racah parameter C. The value of C can be determined by observing forbidden transitions to doublet levels. Such transitions have not been seen in this work because of the low cobalt concentration. The spin-orbit mixing energy between any of the doublet levels and the $^4T_1(^4P)$ level is of the order of the spin-orbit interaction parameter ζ for the free cobalt atom [Ref. 6, p. 77], which is approximately 540 cm^{-1} [Ref. 7, p. 437]. Hence, by perturbation theory, the doublet levels within 2000 cm^{-1} or 2500 cm^{-1} of the quartet level should be quite strongly mixed with that level. The details of the mixing cannot be calculated until the value of C is known. It is possible that some of the structure on the absorption peak is also due to interactions between cobalt atoms and GaP phonons.

The above discussion raises the possibility that the total spin S is not a good quantum number for cobalt in GaP. The value of B for the transition metals in free space and in the crystals studied previously is as large as or larger than the value of the free ion spin-orbit interaction parameter [Ref. 7, p. 437; Ref. 2]. For cobalt in GaP the value of B is less than 60 percent of the free ion spin-orbit interaction parameter. Hence orbit effects should be more important in the spectrum of cobalt-doped GaP than in the spectra studied previously. The matrix elements with spin-orbit effects included are available for the closed-shell d^7 configuration [Ref. 26]. Energy level schemes calculated from the matrices confirm the transition assignments already made and therefore justify the use of S as a good quantum number. The complete matrices cannot be used profitably for a quantitative analysis until there is enough data to determine B, C, Dq, and ζ.

Spin-orbit splitting of the $^4A_2$ and the $^4T_1(^4P)$ levels themselves was a possible explanation of the structure on the upper peak. Calculation shows that the $^4A_2$ level is not split. The splitting of the $^4T_1(^4P)$ level, which depends on the value of Dq/B, is shown in Fig. 32. In the region from Dq/B = 1.8 to 2.1, the splitting should be less than 100 cm^{-1}. Hence spin-orbit splitting of the $^4T_1(^4P)$ level cannot explain the structure. The spin-orbit splitting of the $^4T_1(^4F)$ level is also shown in Fig. 32. For $1.8 \leq Dq/B \leq 2.1$, the splitting should be about 300 cm^{-1}, which is approximately the width of the peak

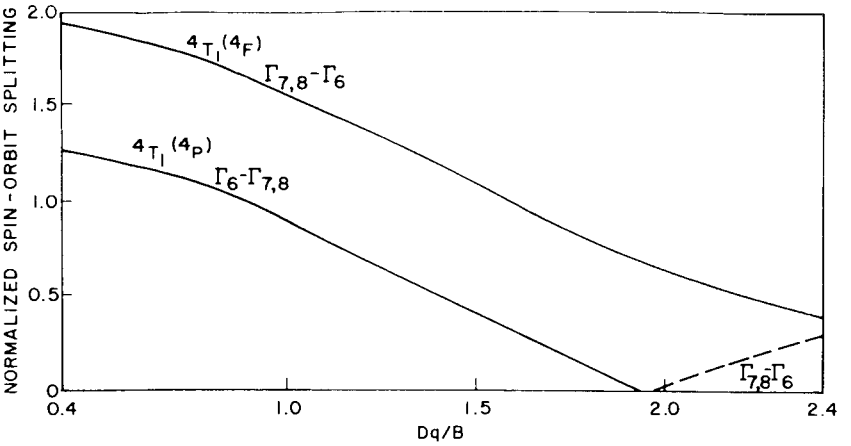

FIG. 32. TOTAL SPIN-ORBIT SPLITTING IN UNITS OF ξ FOR THE $^4T_1(^4F)$ AND $^4T_1(^4P)$ LEVELS VS Dq/B.

centered at 8200 cm^{-1}. Because the peak was so weak, such a width assignment is tentative.

A d^7 configuration is the only d^n configuration for which a fit is possible. The closed-shell restriction may be relaxed to allow the presence of a single s electron (5s, for instance). The presence of an unpaired s electron would increase the total spin S of a configuration but would not change the value of L and hence would not affect the crystal field splittings. However the spectrum for an ion with a partially full p shell as well as a partially full d shell would probably be quite different from that predicted for a d^7 configuration. The matrix elements needed to calculate the level schemes for such ions are not available. Overall, it appears that the observed spectrum should be attributed to a d^7 configuration with all shells, except possibly s shells, closed.

2. Empty Cobalt Levels

The spectrum (Fig. 30) of low-resistance p-type GaP containing zinc and cobalt is not understood. It cannot be explained in terms of either a d^6 configuration or a d^7 configuration. A possible explanation is that the spectrum is due to a configuration with both open d and open p shells. The increase in absorption from about 3.1μ to the band edge may be due to transitions from different parts of the valence

band to the cobalt level. Since the shape of the GaP valence band is not known, this idea cannot be discussed quantitatively. The sharp absorption at 3.45μ is at the correct energy for a transition from zinc to cobalt impurity levels.

D. SUMMARY OF OPTICAL WORK

Structure in the absorption spectrum of GaP containing full cobalt acceptors has been attributed to transitions within the cobalt d shell. It has been determined that the d shell contains seven electrons and that the cobalt is at the center of a tetrahedron. It appears that when the cobalt level is full, crystal field theory provides a quantitatively correct explanation of the d-shell structure. The absorption spectrum observed in material containing empty cobalt acceptors is not understood.

VII. A MODEL FOR COBALT IMPURITIES

The experimental results described in the previous chapters which are needed in the following discussion include the following: (1) Cobalt impurities give rise to a 0.41 eV acceptor level; (2) full cobalt acceptors have a $3d^7$ configuration with all shells, except possibly s shells, full; (3) the absorption spectrum of samples containing empty cobalt acceptors is not understood but may in part be due to cobalt with open p and d shells; (4) although cobalt diffuses interstitially, the final cobalt concentration is apparently controlled by crystal defects. Also needed are the facts that a free cobalt atom has nine electrons outside of an argon core and that a cobalt atom which has accepted an electron has ten outer electrons.

The cobalt in the optical and Hall effect samples could have been on either (a) interstitial sites, (b) substitutional phosphorus sites, or (c) substitutional gallium sites. Possibility (a) is not likely for the following reasons. The optical data show that seven of the ten electrons around a full cobalt acceptor are in the d shell. If the cobalt is on an interstitial site, two of the remaining three electrons can be accommodated in 4s levels and the third electron must go into either a 4p or a 5s level (we can safely neglect higher lying orbits). The presence of a 4p electron is not consistent with the observation of the d^7 spectrum. In the free ion, 5s levels lie approximately 20,000 cm^{-1} above 4p levels so it seems unlikely that the accepted electron would occupy a 5s orbit rather than a 4s orbit. All told, possibility (a) seems quite unlikely. Possibility (b) is unlikely on chemical grounds and would lead to severe electron accounting problems.

The hypothesis that the cobalt is on gallium sites is consistent with all the data. It is also consistent with the suggestion that the cobalt concentration is controlled by crystal defects and with the optical and Hall effect data. Cobalt has one less electron outside of its d shell than gallium. Hence there is an empty bond around cobalt atoms on gallium sites which can accept an electron. When the acceptor level is full, there are seven electrons in the 3d shell and three in s-p bonding orbitals. The presence of full bonding orbitals would not

interfere with the d^7 spectrum. This model for the cobalt impurity is shown schematically in Fig. 33; the energy level scheme of the full cobalt level in Fig. 34 results from this model. It was not possible to determine the energy levels of the empty acceptors from simple crystal field theory. With the simple theory it cannot be shown that the acceptor is due to changes on the d-shell structure. Hence the ionization energy theory as proposed by Allen [Ref. 1] cannot be applied.

A possible explanation of the empty level is that it consists of a d^7 configuration plus an empty bonding orbital. This assumption is consistent with the lack of a crystal field spectrum for the p-type sample. On the basis of this explanation, the electron degeneracy factor for the cobalt level is one-eighth. Also, there should be no strong parity selection rules for optical transitions involving the level. Photoconductivity could be used to check this prediction.

The optical data show that the 0.41-eV level is the only cobalt acceptor level. The same absorption spectrum was seen whenever the Fermi level was above that level. A second acceptor level could arise if cobalt accepted an electron into its d shell or into its 4p or 5s levels. These possibilities are inconsistent with either the observation of the d^7 spectrum or with the spectra of free cobalt ions.

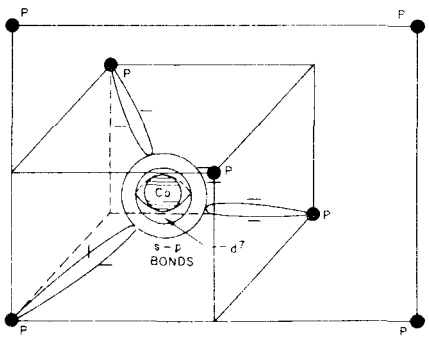

FIG. 33. A SCHEMATIC DRAWING OF A d^7 COBALT ATOM ON A GALIUM SITE. Acceptor level full.

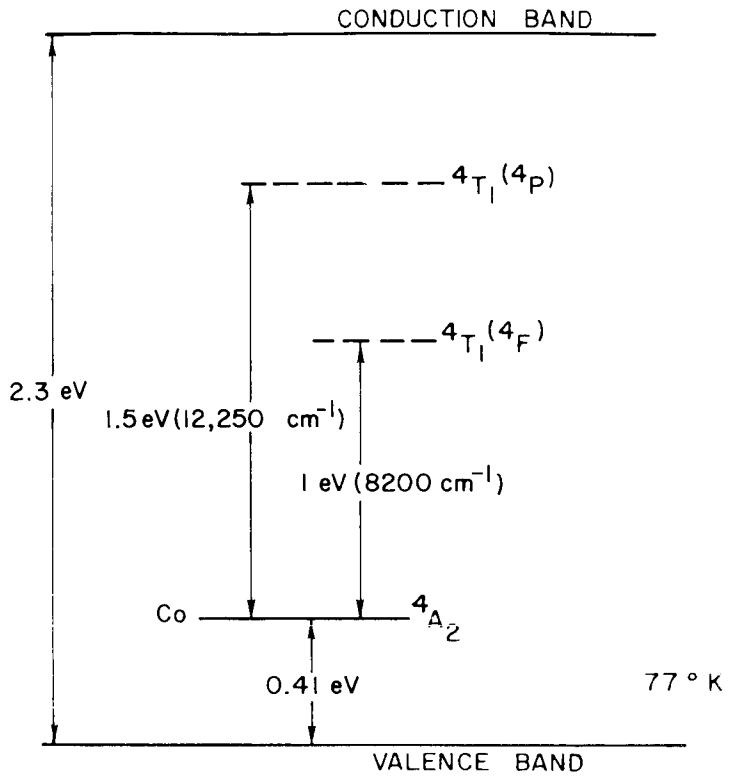

FIG. 34. GROUND AND EXCITED STATES OF COBALT IN GaP AS DETERMINED BY THIS RESEARCH. Cobalt acceptor states full.

VIII. CONCLUSIONS AND SUGGESTIONS FOR FUTURE WORK

A. CONCLUSIONS

Electrical measurements show that cobalt is an acceptor in GaP. Optical transmission data show that the cobalt atom is a substitutional impurity and that when it has accepted an electron it has a $3d^7$ configuration with the s-p bonding orbitals full. The assignment of the cobalt atom to a substitutional site is consistent with the observation, based on diffusion data, that the cobalt concentration was related to the defect density in the crystals.

Crystal field theory has led to a quantitatively correct result in a covalent crystal. The theory allowed the determination of the number of d electrons around full cobalt acceptors. The small value of the Racah parameter B reflects the covalency of GaP. These experimental results are in contrast to the *a priori* notion that crystal field theory should not apply in a covalent material.

The extension of crystal field theory to the calculation of transition-metal impurity ionization energies could not be applied to cobalt in GaP. However, it was possible to construct a model of a transition-metal impurity from a combination of crystal field and Hall effect data. The theory suggested by Allen [Ref. 1] does provide a framework to which the results on cobalt can be related.

B. SUGGESTIONS FOR FUTURE WORK

A photoconductivity study of cobalt-doped GaP, particularly of p-type material, could provide valuable information about the cobalt level. A study of other transition metals in a GaP system would be quite useful. Hopefully such a study could use the diffusion data given in this work. The ionization energy of sulfur impurities and the cobalt concentration in cobalt diffused samples are also suggested as areas for future work.

APPENDIX A. THE SOLUBILITY OF COBALT IN DOPED GaP

The purpose of this appendix is to show that the observed dependence of the cobalt concentration on the crystal used for the diffusion cannot be explained in terms of the initial dopings of the crystals. The arguments below follow those given by Shockley and Moll [Ref. 23].

The theory used here results from the fact that the solubility of a neutral species will not depend on the location of the crystal Fermi level; it may, of course, depend on the temperature, pressure, etc.

Since the data in Chapter V showed that cobalt is an acceptor in GaP, let us restrict ourselves to the theory for a simple acceptor impurity. The total concentration of acceptors is equal to the concentration of negatively charged acceptors N_A^- and the concentration of neutral acceptors N_A^o; that is,

$$N_A = N_A^- + N_A^o \,. \tag{A.1}$$

If the acceptor is diffused into a crystal, N_A^o will depend on the diffusion temperature, overpressure, etc., but it will not depend on the doping of the crystal. For the theory to apply, the diffusion must have been long enough for the acceptor concentrations to have reached their equilibrium values. The quantities in Eq. (A.1) may be related to each other with Fermi factors; that is,

$$N_A^- = N_A^o \exp\left(\frac{E_F - E_A}{kT}\right) \tag{A.2}$$

and

$$N_A = N_A^o \left[1 + \exp\left(\frac{E_F - E_A}{kT}\right)\right] , \tag{A.3}$$

where $E_F - E_A$ is the difference between the acceptor ionization energy and the Fermi energy, and kT is thermal energy at the temperature at which the acceptor was introduced. Qualitatively, Eq. (A.3) predicts that an acceptor should be considerably more soluble in n-type crystals than in p-type crystals. If $E_F < E_A$, then

$$N_A = N_A^o \quad . \tag{A.4}$$

Therefore, N_A^o may be determined by measuring the acceptor concentration in a low-resistance p-type sample. Once N_A^o is known, Eq. (A.3) can be used to calculate N_A for any value of $E_F - E_A$ and hence for any doping. The major difficulty in the application of Eq. (A.3) is that high-temperature values of the quantities needed to calculate $E_F - E_A$ are not generally available.

The theory was applied to the data for cobalt diffused at 1100 °C into GaP. The resulting theoretical curve[†] is compared with the experimental data in Fig. 35. It is clear that the experimental values do not fit on the theoretical curve. In fact, even a qualitative fit is impossible because the concentration in the p-type sample was as large as that in three of the n-type samples. Possible explanations of the lack of agreement between the experimental data and the theory are that cobalt diffuses as a neutral atom and that the cobalt concentration is determined by a nonequilibrium defect concentration in the crystals.

On the basis of Fig. 35, it is concluded that the dependence of the cobalt concentration on the crystal used for diffusion cannot be explained by the initial dopings of the crystals.

[†]The following values were used to calculate the plot: $N_A^o = 2 \times 10^{15}$ cm^{-3}, energy gap = 1.7 eV at 110 °C, $n_i^2 = 2 \times 10^{34}$ cm^{-6}, cobalt ionization energy = 0.41 eV. The value for N_A^o was calculated from the data for $N_d = 2 \times 10^{16}$ cm^{-3} rather than from the p-type data so that the theoretical curve would fit the n-type data reasonably well. Since the purpose of the figure was to show that a fit between theory and experiment was not possible, this step seems justified. The other values used in the calculation are extrapolations from data taken at much lower temperatures.

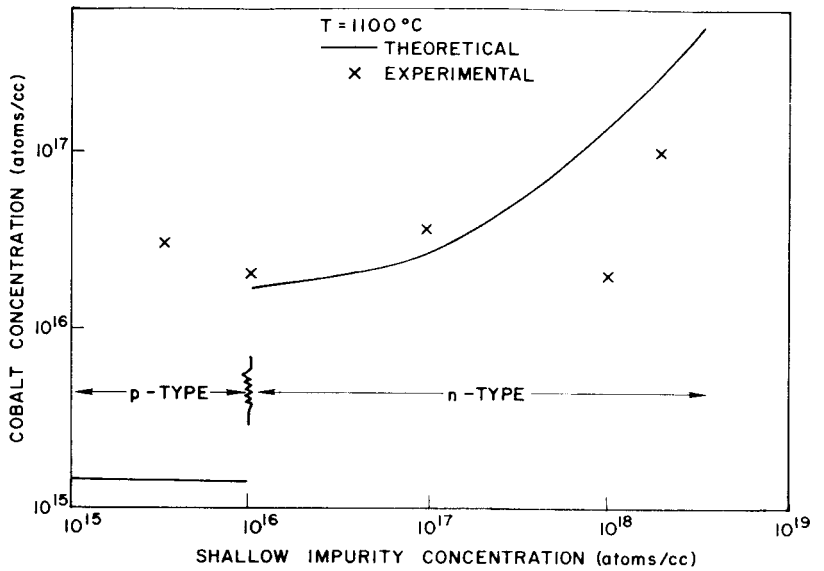

FIG. 35. THEORETICAL AND EXPERIMENTAL DEPENDENCE OF COBALT CONCENTRATION ON INITIAL DOPING.

REFERENCES

1. J. W. Allen, Physics of Semiconductors (Proc. 7th Intern. Conf.) (Dunod, Paris and Academic Press, New York, 1964), p. 781.

2. R. Pappalardo and R. E. Dietz, Phys. Rev., 123, 1188 (1961).

3. H. A. Weakliem, J. Chem. Phys., 36, 2117 (1962).

4. J. C. Slater, Quantum Theory of Atomic Structure (McGraw-Hill Book Company, New York, 1960), vol. 1, p. 210.

5. C. J. Ballhausen, Introduction to Ligand Field Theory (McGraw-Hill Book Company, New York, 1962).

6. D. S. McClure, Electronic Spectra of Molecules and Ions in Crystals (Academic Press, New York, 1959).

7. J. S. Griffith, The Theory of Transition-Metal Ions (University Press, Cambridge, 1962).

8. M. Tinkham, Group Theory and Quantum Mechanics (McGraw-Hill Book Company, New York, 1964), p. 329.

9. Y. Tanabe and S. Sugano, J. Phys. Soc. (Japan) 9, 753 (1954). Also given in D. S. McClure, Part II, Chapter 1.

10. W. Shockley and J. T. Last, Phys. Rev., 107, 392 (1957).

11. J. F. Gibbons and P. C. Prehn, "Epitaxial Vapor Growth of III-V Compounds," Rept. SEL-63-105 (TR No. 4711-1), Stanford Electronics Laboratories, Stanford, Calif., Oct 1963.

12. Yen-sun Chen, "Lattice Vibration Spectra of $GaAs_xP_{1-x}$ Single Crystals," Rept. SEL-65-092 (TR No. 5108-1), Stanford Electronics Laboratories, Stanford, Calif., Oct 1965.

13. H. C. Gatos and M. C. Levine, "Chemical Behavior of Semiconductors, Etching Characteristics," TR No. 293, Lincoln Laboratories, M.I.T., Cambridge, Mass., Jan 1963 (Etchant No. 12), p. 39.

14. O. Madelung, Physics of III-V Compounds (John Wiley & Sons, New York, 1964), p. 223.

15. E. H. Putley, The Hall Effect and Related Phenomena (Butterworths & Co., London, 1960), p. 124.

16. H. C. Montgomery and W. L. Feldman, J. Appl. Phys., 36, 3228 (1966).

17. R. N. Hall and J. H. Racette, J. Appl. Phys., 35, 3079 (1964).

18. J. T. Edmunds, J. Appl. Phys., 31, 1428 (1960).

19. J. W. Allen and G. L. Pearson, "Ternary Phase Diagrams for the Ga-P-Zn and Ga-As-Zn Systems with Applications to Diffusion Problems," Rept. SEL-65-053 (TR No. 5109-1), Stanford Electronics Laboratories, Stanford, Calif., May 1965.

20. C. P. Thurmond and C. J. Frosch, J. Electro. Chem. Soc., 111, 184 (1964).

21. R. T. Overman and H. M. Clark, Radioisotope Techniques, (McGraw-Hill Book Company, New York, 1960), p. 117.

22. B. I. Boltaks and F. S. Shishiyanu, Soviet Phys.-Solid State, 5, 1680 (1964).

23. W. Shockley and J. L. Moll. Phys. Rev., 119, 1480 (1960).

24. H. R. Potts, "Electron Microprobe Studies of Lattice-Point Defects in Semiconductor Crystals," Rept. SEL-64-075 (TR No. 5106-2), Stanford Electronics Laboratories, Stanford, Calif., Jul 1961.

25. J. W. Allen and R. J. Cherry, J. Chem. Phys. Solids, 123, 163 (1962).

26. J. C. Eisenstein, J. Chem. Phys., 34, 1628 (1961).

UNCLASSIFIED

Security Classification

DOCUMENT CONTROL DATA - R&D

(Security classification of title, body of abstract and indexing annotation must be entered when the overall report is classified)

1. ORIGINATING ACTIVITY *(Corporate author)*
Stanford Electronics Laboratories
Stanford, California

2a. REPORT SECURITY CLASSIFICATION
UNCLASSIFIED

2b. GROUP

3. REPORT TITLE
A CRYSTAL FIELD ANALYSIS OF COBALT IMPURITIES IN GaP

4. DESCRIPTIVE NOTES *(Type of report and inclusive dates)*
Technical Report, December 1966

5. AUTHOR(S) *(Last name, first name, initial)*
Loescher, Douglas H.

6. REPORT DATE	7a. TOTAL NO. OF PAGES	7b. NO. OF REFS
October 1966	62	26

8a. CONTRACT OR GRANT NO.	9a. ORIGINATOR'S REPORT NUMBER(S)
Research Grant No. NsG-555	TR No. 5109-2
b. PROJECT NO.	
c.	9b. OTHER REPORT NO(S) *(Any other numbers that may be assigned this report)*
d.	SEL-66-087

10. AVAILABILITY/LIMITATION NOTICES
Reproduction in whole or in part is permitted for any purpose of the United States Government.

11. SUPPLEMENTARY NOTES	12. SPONSORING MILITARY ACTIVITY
	National Aeronautics and Space Administration

13. ABSTRACT Crystal field theory has been used to explain the electrical and optical properties of cobalt-doped GaP. In n-type GaP, cobalt gives rise to optical absorption bands at 0.8 and 1.25 microns. From Hall effect data it has been found that cobalt is a deep acceptor with an ionization energy of 0.41 eV. A crystal field analysis has shown that the electron configuration around full cobalt acceptors (negatively charged) consists of seven d-electrons with all other electrons in closed shells and furthermore, that cobalt atoms have substituted for gallium atoms in the lattice. In general, the analysis has shown that crystal field theory can be used to obtain detailed electron models of semiconductor impurities.

In the course of the study, methods were developed to grow epitaxial single crystals of GaP doped with either sulfur or zinc. Predictable sulfur dopings between 6×10^{16} and 4×10^{18} cm^{-3} were achieved. Radiotracer diffusions were used to introduce a known concentration of cobalt into the samples used for optical and electrical measurements. Diffusion data show that the cobalt diffused both substitutionally and interstitially. The data suggest that the cobalt concentration after diffusion was determined by a nonequilibrium density of crystal defects. This hypothesis is consistent with the conclusion from the optical data that the cobalt was on gallium sites.

DD FORM 1 JAN 64 1473

UNCLASSIFIED

Security Classification

14. KEY WORDS	LINK A		LINK B		LINK C	
	ROLE	WT	ROLE	WT	ROLE	WT
SOLID STATE						
COBALT DIFFUSION IN GALLIUM PHOSPHIDE						
ELECTRICAL AND OPTICAL PROPERTIES OF COBALT IN GALLIUM PHOSPHIDE						
CRYSTAL FIELD THEORY IN GALLIUM PHOSPHIDE						

INSTRUCTIONS

1. ORIGINATING ACTIVITY: Enter the name and address of the contractor, subcontractor, grantee, Department of Defense activity or other organization *(corporate author)* issuing the report.

2*a*. REPORT SECURITY CLASSIFICATION: Enter the overall security classification of the report. Indicate whether "Restricted Data" is included. Marking is to be in accordance with appropriate security regulations.

2*b*. GROUP: Automatic downgrading is specified in DoD Directive 5200.10 and Armed Forces Industrial Manual. Enter the group number. Also, when applicable, show that optional markings have been used for Group 3 and Group 4 as authorized.

3. REPORT TITLE: Enter the complete report title in all capital letters. Titles in all cases should be unclassified. If a meaningful title cannot be selected without classification, show title classification in all capitals in parenthesis immediately following the title.

4. DESCRIPTIVE NOTES: If appropriate, enter the type of report, e.g., interim, progress, summary, annual, or final. Give the inclusive dates when a specific reporting period is covered.

5. AUTHOR(S): Enter the name(s) of author(s) as shown on or in the report. Enter last name, first name, middle initial. If military, show rank and branch of service. The name of the principal author is an absolute minimum requirement.

6. REPORT DATE: Enter the date of the report as day, month, year; or month, year. If more than one date appears on the report, use date of publication.

7*a*. TOTAL NUMBER OF PAGES: The total page count should follow normal pagination procedures, i.e., enter the number of pages containing information.

7*b*. NUMBER OF REFERENCES: Enter the total number of references cited in the report.

8*a*. CONTRACT OR GRANT NUMBER: If appropriate, enter the applicable number of the contract or grant under which the report was written.

8*b*, 8*c*, & 8*d*. PROJECT NUMBER: Enter the appropriate military department identification, such as project number, subproject number, system numbers, task number, etc.

9*a*. ORIGINATOR'S REPORT NUMBER(S): Enter the official report number by which the document will be identified and controlled by the originating activity. This number must be unique to this report.

9*b*. OTHER REPORT NUMBER(S): If the report has been assigned any other report numbers *(either by the originator or by the sponsor)*, also enter this number(s).

10. AVAILABILITY/LIMITATION NOTICES: Enter any limitations on further dissemination of the report, other than those imposed by security classification, using standard statements such as:

(1) "Qualified requesters may obtain copies of this report from DDC."

(2) "Foreign announcement and dissemination of this report by DDC is not authorized."

(3) "U. S. Government agencies may obtain copies of this report directly from DDC. Other qualified DDC users shall request through _____."

(4) "U. S. military agencies may obtain copies of this report directly from DDC. Other qualified users shall request through _____."

(5) "All distribution of this report is controlled. Qualified DDC users shall request through _____."

If the report has been furnished to the Office of Technical Services, Department of Commerce, for sale to the public, indicate this fact and enter the price, if known.

11. SUPPLEMENTARY NOTES: Use for additional explanatory notes.

12. SPONSORING MILITARY ACTIVITY: Enter the name of the departmental project office or laboratory sponsoring *(paying for)* the research and development. Include address.

13. ABSTRACT: Enter an abstract giving a brief and factual summary of the document indicative of the report, even though it may also appear elsewhere in the body of the technical report. If additional space is required, a continuation sheet shall be attached.

It is highly desirable that the abstract of classified reports be unclassified. Each paragraph of the abstract shall end with an indication of the military security classification of the information in the paragraph, represented as *(TS)*, *(S)*, *(C)*, or *(U)*.

There is no limitation on the length of the abstract. However, the suggested length is from 150 to 225 words.

14. KEY WORDS: Key words are technically meaningful terms or short phrases that characterize a report and may be used as index entries for cataloging the report. Key words must be selected so that no security classification is required. Identifiers, such as equipment model designation, trade name, military project code name, geographic location, may be used as key words but will be followed by an indication of technical context. The assignment of links, roles, and weights is optional.